Chapter 4

Surface alloys and alloy surfaces: the platinum-tin system

Sylvia Speller[a] and Ugo Bardi[b]

[a] Research Institute for Materials, University of Nijmegen,
Toernooiveld 1, 6525 ED Nijmegen, The Netherlands

[b] Dipartimento di Chimica, Università di Firenze,
Via G. Capponi 9 – 50014 Firenze, Italy, bardi@unifi.it

1. INTRODUCTION

The effect of the surface structure and composition on the properties of metals and alloys has been recognized since the early times of metallurgy. Considering noble metals, the use of diffusion phenomena in bimetallic systems has a history that goes back to very early times in human history, when "fire gilding" techniques using mercury - gold alloys (amalgams) were developed. In recent times, noble metal alloys are extensively used in fields such as heterogeneous catalysis, where a large number of catalysts are multimetallic and contain at least one noble metal species [1, 2, 3]. The properties of the surface of noble metal alloys also find application in a variety of different fields, at first sight not related to surface science, for instance in thermal barrier systems where platinum aluminides are used as intermediate materials acting as corrosion barriers in high temperature environments [4].

The general field of the surface structural properties of bimetallic systems has been reviewed by Bardi [5] and more recently for the specific field of ordered systems by Vasiliev [6]. The theoretical factors leading to ordering and reconstruction at binary alloy surfaces have been recently reviewed by Treglia et al [7]. Another general review on the properties of bimetallic surfaces was reported by Rodriguez [8] and a general assessment of the factors leading to surface alloying has been published by Christensen et al [9]. The present paper is dedicated to a review of the state of the art of the knowledge of the surface composition and atomic level structure for platinum alloys and for one specific noble metal alloy, the Pt-Sn system, which has been extensively studied during the last few years.

In general, noble metals alloyed with metals of the left rows of the periodic table produce compounds with highly negative enthalpy of formation which very often form ordered intermetallic compounds, a fact already noted some time ago [10] and which more recently has been related to electron exchange among the species involved [11]. These compounds form a class of materials which gives rise to a wealth of surface phenomena. Among these phenomena we can cite the formation of ordered 2D ("two-dimensional") phases, "sandwich" surface layers, and long range undulations formed by lattice mismatch in turn due to the variations of the lattice constant resulting from composition variations. Platinum alloys and bimetallic systems are especially important in catalysis. Platinum-tin alloys are specifically important as catalytic electrode materials for direct methanation fuel cells (DMFC) [12] and as catalysts for naptha reforming and hydrogenation/dehydrogenation reaction of hydrocarbons, where the addition of tin to Pt supported catalysts decreases coke formation and increases lifetime and selectivity [13].

The Pt-Sn system has a highly negative enthalpy of alloying and gives rise to ordered bulk phases [14]. One of these phases (Pt_3Sn) is cubic (symmetry $Pm3m$, $AuCu_3$ type). This phase, as well as the phases obtained by depositing tin on pure platinum surfaces, have been examined by the full array of the available structure sensitive surface science techniques: diffraction methods (e.g ion scattering ALISS, low energy electron diffraction LEED and X-ray photoelectron diffraction, XPD) and scanning tunneling microscopy (STM). By using these techniques it has been possible to determine the atomic coordinates of the species present within the first few layers of the surface for different orientations and chemical compositions. It has been also possible to evidence complex phenomena of surface reconstruction and of formation of mesoscopic surface features. The present paper will summarize and review the results obtained and compare them with the data available for other ordering alloys.

2. METHODS

A rapid survey of the methods utilized for the study of binary alloys, and specifically for the Pt-Sn system will be reported here. In the present review, we consider only studies performed in conditions of ultra high vacuum (UHV), where bimetallic Pt-Sn surfaces are stable. It is known that in air and in general in the presence of oxygen at pressures larger than ca. 10^{-6} Torr, tin alloyed with platinum tends to oxidize and de-alloy to form oxide phases, a phenomenon that will not be treated here.

In all studies considered here the samples examined were either single crystal alloys of Pt_3Sn composition prepared by melting and zone refining in

vacuum, or surfaces obtained depositing metallic tin on single crystal pure Pt substrates. The deposition was performed in UHV conditions using thermal evaporation sources. The substrates always needed a specific cleaning procedure in vacuum, which was obtained by noble gas ion bombardment (or "sputtering") for the purpose of removing adsorbed impurity and oxide layers and for flattening the surface, i. e. reducing the surface roughness. The sputtering treatment was normally followed by annealing, still in vacuum, for the complete smoothing and equilibration of the surface under study.

In the study of the surface phases of the Pt-Sn system, as well as of other binary systems, a variety of experimental methods are available. Surface spectroscopies based on ion or electron interaction with the surface provide composition information with a depth resolution that can go from a few atomic layers (X-ray photoelectron spectroscopy, XPS and Auger electron spectroscopy, AES) to single atomic layer resolution. The latter can be obtained by low energy ion scattering (LEIS) a method which has been extensively used for the study ot the Pt-Sn system. Since surface spectroscopic methods are rather well known we will not review them in detail here.

In terms of *structural information*, that is the determination of the atomic coordinates of at least some of the species in the surface region, several methods are available. We can class these methods in two main groups: scattering techniques (ion and electron) and scanning probe techniques. In several cases - and specifically for the Pt-Sn system - a combination of these methods can provide the complete determination of the crystallographic parameters of the first 2-3 atomic planes of a surface. The surface phases observed in the Pt-Sn system are normally termed in reference to their in-plane periodicity, as observed most often by LEED. For a description of this method and for notes about how the surface crystallographic conventions need to be somewhat modified when applied to the field of alloy surfaces, see the appendix to the present paper.

Here, we will briefly describe the surface structural methods extensively used for the Pt-Sn system.

– *Electron diffraction,* Low energy electron diffraction (LEED) is the oldest and still the most widely applied crystallographic technique used for the determination of the structure of ordered solid surfaces. It is based on the diffraction process that a monoenergetic electron beam (ca. 20-500 eV) undergoes when interacting with a surface. On well ordered, single crystal surfaces long range interference of the scattered electrons leads to the formation of a diffraction pattern from which the surface unit mesh can be determined. More information can be extracted from the intensity of each spot as a function of the electron energy and comparing the results with a theoretical calculation. This procedure is defined in the literature as 'dynamical' or "quantitative" LEED analysis, or

as LEED I-V analysis, where "I-V" stands for "Intensity vs. Potential" (see, for instance, [15]). From a comparison of measured and calculated I-V curves it is possible to determine a model of the surface structure with an accuracy of the determination of interatomic distances that may be of the order of 0.01 Å. The sensitivity to composition in LEED is highest when the atomic species have significantly different scattering factors. In favorable cases (e.g. Pt-Ni, [16], the sensitivity to composition has been estimated to extend to a depth of approximately 5 Å from the surface. When the difference in atomic number - and hence in the electron density - is not so large, the sensitivity to composition worsens considerably. However, a composition profile for the first 2-3 atomic layers from the topmost surface could still be obtained for transition elements in adjacent rows of the periodic table, such as the Pt-Sn system considered here [17]. In LEED it is also possible to analyse the angular distribution of the intensity of single diffracted beams (spot profile analysis LEED, SPA-LEED) in order to obtain information on the domain structure of the surface under study, as it has been done for the $Pt_3Sn(111)$ surface [18]. Some studies by electron diffraction of the Pt-Sn system have also been performed by reflected high energy electron diffraction (RHEED) which uses a grazing incidence high energy electron beam. This method can provide information on structural features, such as mesoscopic multilayer "islands" which are difficult to study by LEED.

– *Photoelectron diffraction methods,* PD. These methods are based on the photon stimulated emission of core level electrons from the atomic species in the surface region. These electrons undergo scattering when interacting with the atoms around the emitter. Interference effects cause a variation in the intensity of electron emission as a function of angle or of energy. Measuring this variation it is possible to obtain information about the local structure around the emitting atom. A common set up for PD uses a conventional photon source in the soft X-ray domain (Al Kα or Mg Kα). In this version, the photoelectron intensities are measured for variable angles and the technique goes under the name of XPD (X-ray photoelectron diffraction). As the electrons examined are of relatively high energies (several hundreds of eV), the scattering process is dominated by what is called the 'forward focusing' effect [19]. This effect enhances the intensity of electrons emitted along directions that correspond to densely packed atomic rows and it may be exploited to obtain an immediate qualitative interpretation of the data. Calculations assuming varying degrees of approximation [19] can be used to fit XPD data to a detailed surface structural model. The technique has a larger probing depth than LEED and has the further advantage of being species sensitive, but it is scarcely sensitive to the structure of the topmost surface layer. XPD techniques have been extensively used for the Pt-Sn system, mainly for the study of phases obtained depositing tin on bulk

Pt substrates. All the results reported here for the Pt/Sn system were obtained using a multichannel hemispherical electron analyzer and a conventional, non monochromatized, Mg Kα or Al Kα photon source. Unless otherwise specified, the experimental data were analyzed by means of the single scattering cluster - spherical wave (SSC-SW) model.

– *Ion scattering,* IS. This term indicates a family of related techniques of which the relevant ones here are low energy ion scattering (LEIS) and alkali ion scattering spectroscopy (ALISS). The former, LEIS, is normally used for surface composition analysis with a depth resolution of the order of a single atomic layer, the latter (ALISS) can also provide structural information. Both LEIS [20, 18] and ALISS [21, 22, 23] have been extensively used in the study of Pt-Sn system. In ALISS a beam of low energy ions (typically Li^+) is directed at the surface. The backscattered ions are analyzed in energy and angle. Alkali metals here have a definite advantage over noble gas ions (e.g. He^+ commonly used in LEIS) in the fact that the neutralization probability is much lower. Typically, for helium only about 1-10% of the ions is not neutralized, whereas for lithium the fraction is as high as 50-80% As obvious, the lower neutralization cross section leads to a much better signal to noise ratio. In ALISS (and in LEIS as well) the energy loss due to the elastic collision of the ion with species of the surface is characteristic of the mass of the target atoms and therefore provides compositional information. Structural information, that is information about the relative position of the scatterers at the surface can be obtained using the "shadow cone" associated with the target atom. Calculating the theoretical shadow cone at a given ion energy it is possible to determine a structural model of the surface by a polar angle scan [24]. The use of this method specifically for alloy surfaces and surface alloys has been reviewed by O'Connors et al [25].

– *Scanning Probe Methods* (SPM). Scanning probe techniques are based on the interaction of a sharp tip with the surface under study. This interaction may involve the passage of current by tunneling effect (STM, scanning tunneling microscopy), the measurement of the force between the tip and the surface (AFM, atomic force microscopy) or other physical phenomena. In many cases these techniques provide atomic resolution images of the topmost layer of the surface under study. Of these, STM is at present the most used for the study of metal and alloy surfaces, and atomic resolution has been attained in studies performed in vacuum on samples cleaned by standard treatments. For the studies discussed here on Pt_3Sn surfaces an Omicron STM-1 system has been used housed in an UHV system. The base pressure in the STM chamber was kept in the 10^{-11} Torr range.

With respect to surface roughness STM is rather 'touchy' in comparison to structural analysis methods such as LEED. LEED is a relatively long range

method averaging over the coherence length (ca. 200 Å) of the electrons whereas STM is a short range order method with atomic resolution. On a rough surface good tip-surface contact is hard to achieve and, in the worst case, tip damage is likely to occur. With respect to surface cleanliness STM is as sensitive as field ion microscopy (FIM), i. e. very low levels of impurities are detectable albeit not identifiable. Furthermore, rather low levels of impurities, in some cases below the detection limits of AES, lead to a deterioration of the STM tip which may pick up such impurities. The Pt-Sn samples used in the studies discussed here were found to give rise to no impurity segregation phenomena, hence to provide a relatively "easy" system. The final control of the sample quality is, however, the STM topography. All STM topographs reported here were measured at room temperature in the constant current mode. The lateral coordinates were calibrated using the atomically resolved surfaces of Si(111)(7x7) and Pt(110)(1x2). The vertical scale was calibrated at atomic steps on surfaces.

In the case of the STM studies of low-index Pt_3Sn surfaces the results obtained are in some respects textbook examples: compared to other alloys the chemical contrast observed by STM is large ($z_{Pt} - z_{Sn} \approx 50$ pm). Much lower values (of the order of 10 pm) were observed with other Pt-alloys [26]. Also the sign of the corrugation varies with the alloy composition: Pt is measured as a protrusion in the Sn-Pt and Co-Pt systems, but as a depression in PtNi and PtRh. The chemical contrast can have different origins. In most cases a difference in the electronic density of states at the two species is responsible. Although chemical discrimination is achieved on very local scale the chemical contrast is partly disturbing because the STM "topography" is polluted by the electronic effects, a similar effect is observed on semiconductor surfaces, eg. Si(111). However, the variation of the contrast with gap voltage is relatively low with Pt-Sn surfaces. Another reason for chemical contrast can be a different interaction of the tip with the two elements on the surface. Additionally, this interaction can be mediated by a molecule or adsorbate at the tip which can be observed by means of sudden contrast changes during the scans. Since the characterization of the tip is a long-standing problem in STM the details of this kind of contrast formation are not known at present. However, the Pt-Sn contrast is never observed together with tip changes, such that one may attribute the contrast to the differences in the electronic density of states [27]. One is tempted to relate the tendency of a system to chemical order with the corrugation amplitude in the chemical contrast, because systems with lower chemical order, most often also show lower chemical contrast (e.g. Au_3Pd, [28]) and vice versa. It is interesting to note that STM is not the only method leading to local chemical contrast. Also in field ion microscopy a local tunnel process is exploited, however in a much

larger field and chemical discrimination was obtained quite early with Pt-Co surfaces [29].

3. THE PLATINUM–TIN SYSTEM

Pt and Sn form highly exothermic bulk alloys. The phase diagram of the Pt-Sn system is described in detail in [14] (Fig. 1). Two stable intermetallic phases exist: Pt_3Sn and PtSn. Of these, Pt_3Sn has an enthalpy of formation of -50.2 KJ/mol, a melting point of 1675 K and a cubic face centered structure which is sometimes described in the literature using the metallurgical notation $L1_2$. The structure of Pt_3Sn is the same as that of the "prototypical" ordered binary alloy, Cu_3Au, the first binary alloy to have been studied for its surface properties in ultra-high vacuum conditions. The PtSn phase is hexagonal and ordered ($P63/mmc$) with an enthalpy of formation reported as -58.6 KJ/mol and a melting point of 1549 K. Other phases with a definite stoichiometry are reported to exist [14] but only the Pt_3Sn phase has been studied in terms of surface properties.

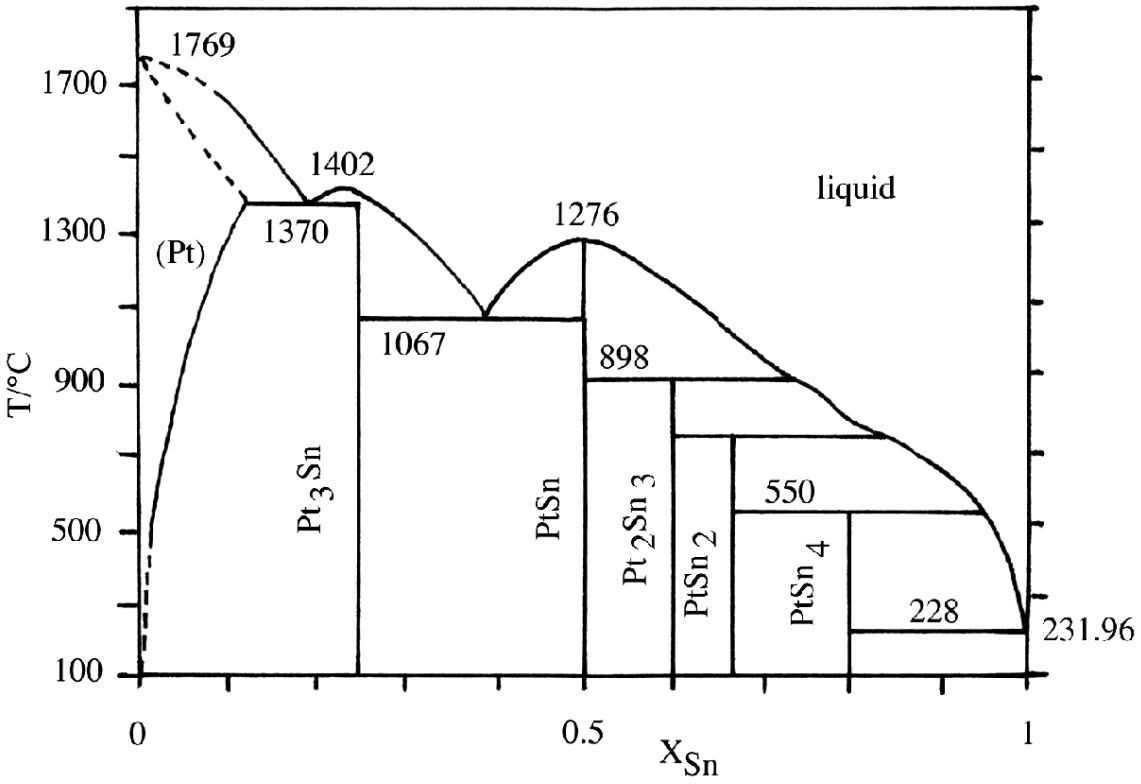

Figure 1: Phase diagram of Pt-Sn after Ref. [14].

3.1 Low index surfaces of the Pt_3Sn alloy

The possible "bulk termination" structures for the Pt_3Sn ordered alloy are shown in Fig. 2. We summarize here the results obtained for the low index surfaces of the Pt_3Sn alloy as a function of the annealing temperature. In the following, we will examine in detail the results for each face.

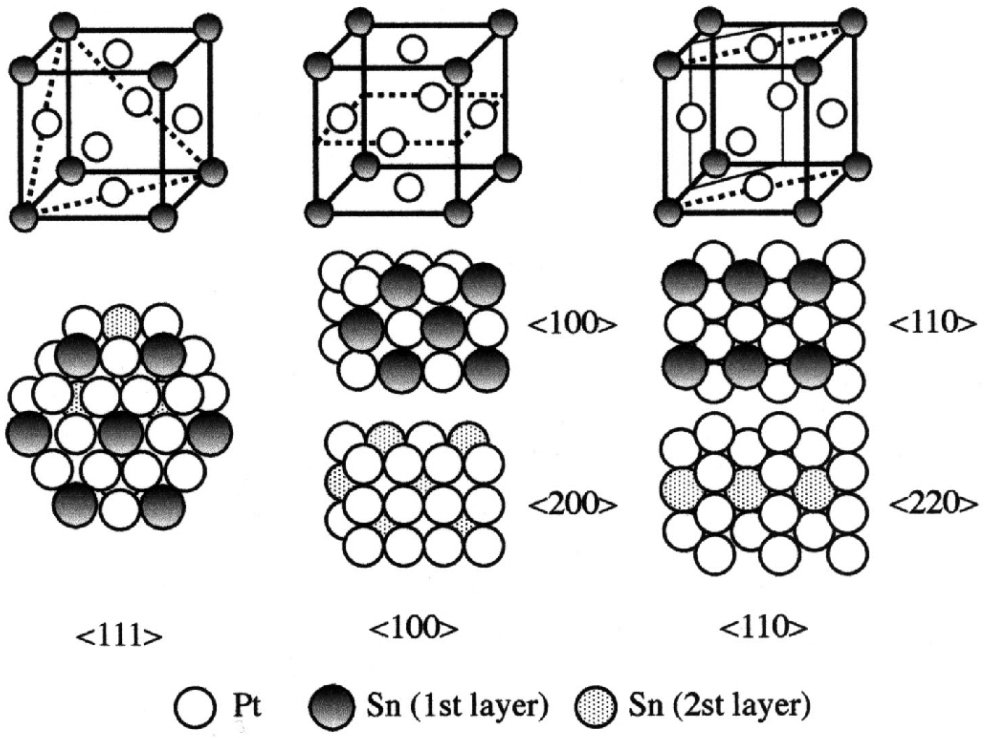

Figure 2: Structure of the Pt_3Sn alloy and low index terminations, after Ref. [30].

3.1.1 $Pt_3Sn(111)$

This surface is the most extensively studied in the Pt_3Sn system. It shows interesting phenomena of bulk-surface equilibrium in the interplay of the two surface phases observed: the $(\sqrt{3} \times \sqrt{3})$ R30°and the p(2x2), with the former stable only in the absence of subsurface tin. Here, we will report in some detail the results of the studies performed.

The first reports on the surface structure of Pt_3Sn were based on qualitative LEED observations and on LEIS results [20, 30, 31, 32]. In these initial studies only the presence of the p(2x2) "bulk periodicity" phase was reported. The atomic structure of this surface was studied by Atrei et. al [17] by quantitative LEED and found to correspond indeed to a simple bulk termination model. The other possible termination, the $(\sqrt{3} \times \sqrt{3})$ R30°, was reported and studied in detail by Atrei et al. [33] who also determined the atomic structure by means of quantitative LEED and found it to correspond to a single layer surface alloy.

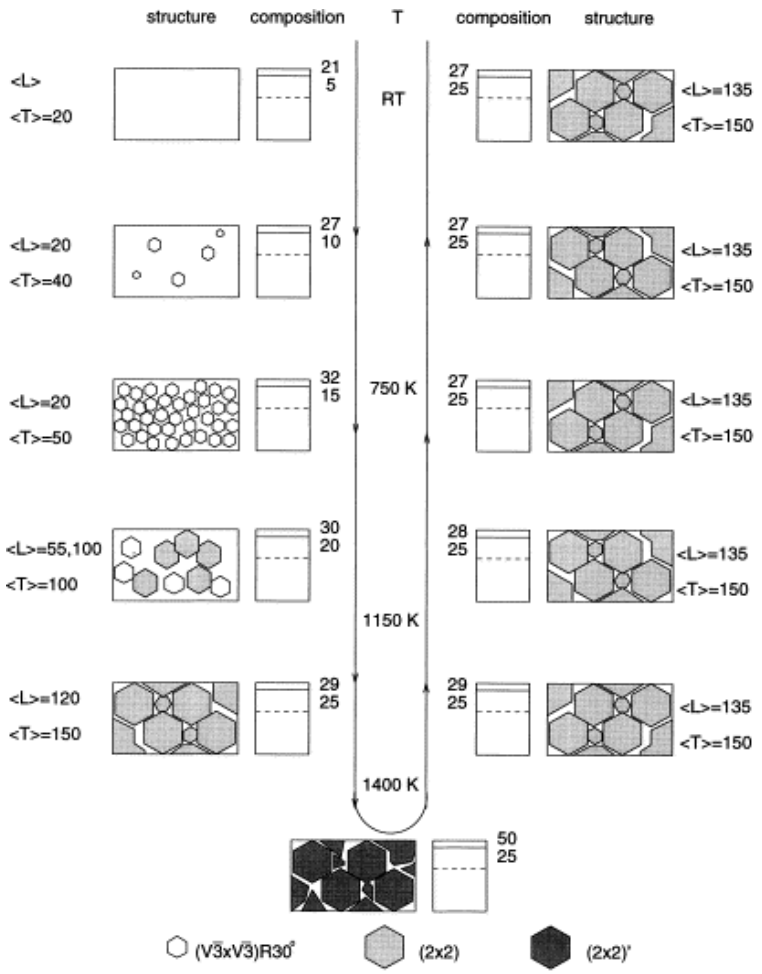

Figure 3: Schematic overview of the surface morphology and the surface composition and altered layer composition on $Pt_3Sn(111)$ as a function of the anneal temperature and history .The figure follows both the increasing temperature trajectory (left side, going down) and the cooling trajectory (right side, going up). $\langle L \rangle$ represents the average domain size of the dominating surface reconstruction, and $\langle T \rangle$ represents the average terrace size. The shape of the reconstructed domains is drawn arbitrarily. The numbers for composition reflect the outermost layer composition (top) and the altered layer composition (bottom). From Ref. [18].

The interplay of the two phases on the $Pt_3Sn(111)$ surface has been object of an extensive study carried out by Ceelen et al. [18] who used mainly a combination of LEIS and SPA-LEED, also carrying the sample at higher temperatures than those attained in the previous studies. A wealth of temperature dependent phenomena was observed in this study concerning bulk-surface chemical equilibrium, domain size variation and phase transitions. The main conclusions that can be drawn from these combined structural and compositional studies is that the $(\sqrt{3} \times \sqrt{3})$ R30° reconstruction is stabilized by the depletion of tin in the subsurface layers and that this depletion is caused by a the combination of sputtering and high temperature annealing (Fig. 3).

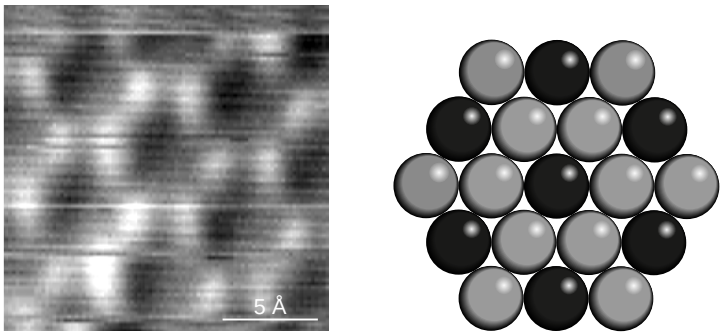

Figure 4: $(17\text{Å})^2$ high-resolution STM image of the $Pt_3Sn(111)$ surface (U_t=0.9V, I_t=1.0nA) and hard-sphere model of the $(\sqrt{3}\times\sqrt{3})$ R30° structure, as derived by crystallographic LEED [34]. Due to some drift the image is slightly elongated in the vertical direction. Pt corresponds to regions of high tunnel current (bright areas), Sn corresponds to regions of low tunnel current (dark areas). From Ref. [35].

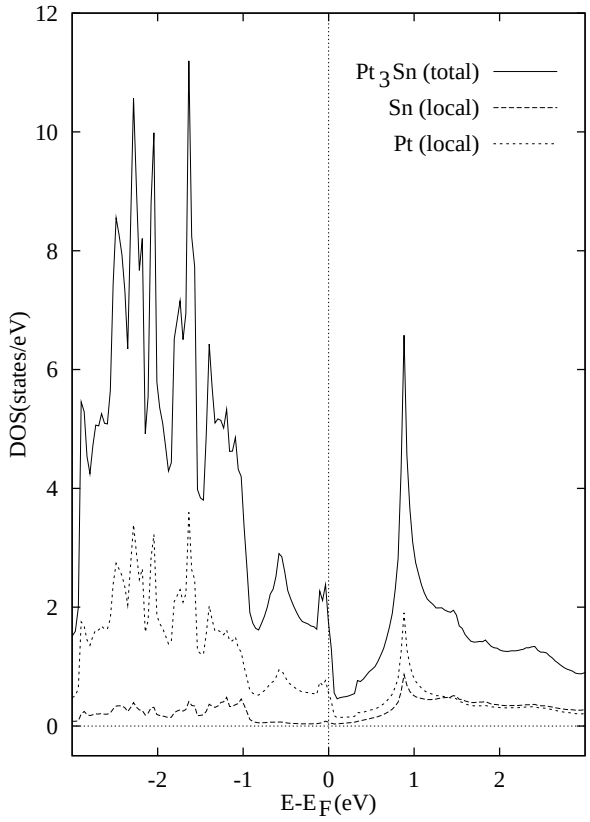

Figure 5: Total (per unit cell) and local (per space-filling atomic spheres of equal size at both Pt and Sn sites) densities of states of Pt_3Sn, calculated by the tight-binding linear muffin-tin orbitals method. At positive (sample-) bias voltages the unoccupied states above E_F are imaged in the STM. From Ref. [27].

A highly detailed picture of the structure of the $Pt_3Sn(111)$ surface in its two possible phases could be obtained by STM [35]. The STM studies were preceded and complemented by studies carried out in the same vacuum chamber by means of LEED, AES and RHEED. In these studies, the depletion of Sn in the near surface layers of the sample resulting by room temperature ion bombardment was confirmed by AES, in agreement with previous studies [34, 18]. Depending on the annealing temperature and annealing time the LEED patterns shows an increasing admixture of the p(2x2) pattern which is the final pattern after annealing to 1000 K. Here, the AES results confirmed the equilibration of the surface composition to reach the expected bulk value.

The STM topographs taken in constant current mode of the $(\sqrt{3}\times\sqrt{3})$ R30° surface confirm the the LEED analysis [33] (Fig. 4) [35]. The bright spots in the topograph are regions of high tunnel current and can be identified as Pt atoms. This interpretation is supported by calculations of the local density of states (LDOS) of Pt_3Sn (Fig. 5)[27]. The LDOS of Sn electronic states is considerably lower at the Fermi-edge compared to the LDOS of Pt. Hence, since STM samples the LDOS essentially, Pt sites should give rise to a larger tunneling

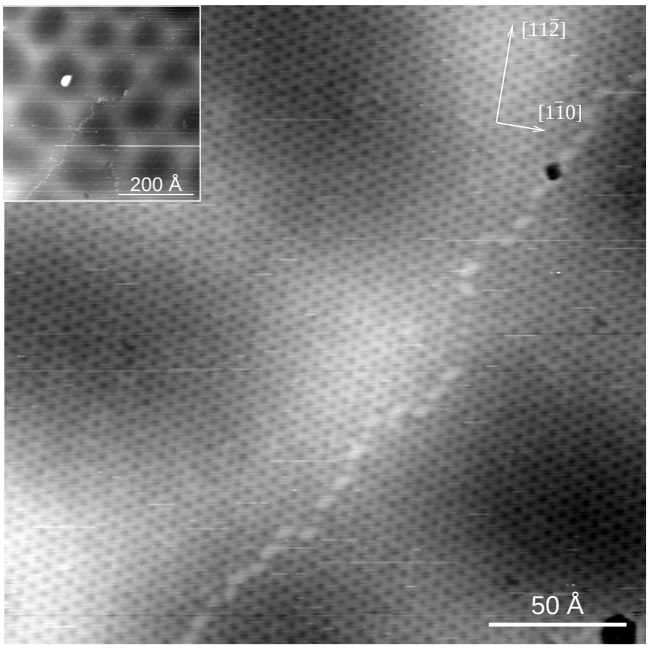

Figure 6: STM-images of the $(\sqrt{3}\times\sqrt{3})$ R30° structure on the $Pt_3Sn(111)$ surface observed after annealing to 600K, a) U_t=0.1V, I_t=0.5nA. The inset shows a (530Å)^2 terrace with the quasi-hexagonal honeycomb-network. The main image is a close-up view of the inset's lower left region, size (236Å)^2. Both the atomic structure and the height modulation due to the honeycomb-network are visible. The irregular line running from the lower left to the upper right corner is a domain wall separating two different $(\sqrt{3}\times\sqrt{3})$ R30°-domains. It shows a defect in the upper right region. From Ref. [35].

current. The contrast between Pt and Sn atoms in these topographs is independent of the tunneling conditions, for variable tunneling currents from 0.5 to 3.0 nA and gap voltages from $\pm$(0.1 to 0.9) V. A large area scan of the same (111) sample surface as in Fig. 6 reveals a further feature [35], i. e. the formation of the so called 'honeycomb' network (Fig. 6). The honeycomb network can be attributed to misfit dislocations due to the Sn depletion in the near surface region as it will be discussed more in detail later on.

After the thermal equilibration obtained by annealing at high temperature a good p(2x2) LEED pattern develops and large terraces are observed with STM (Fig. 7). However, the terraces are mixed, i. e. some terraces are indeed p(2x2) but there remain a few $(\sqrt{3}\times\sqrt{3})$ R30° patches with their honeycomb network. The p(2x2) areas are atomically flat. The p(2x2) areas are decorated with features too large to be single atoms. In a smaller area scan (Fig. 8) a height scan is taken across one of these white features. The height is approximately 2 Å and the width of the order of 10 Å corresponding to a sizeable atomic cluster mono-atomic in height. The clusters are weakly bound, evidence for that is the dragging of clusters across the surface as seen in Fig. 8 for two examples at the left hand side (fuzzy double protrusions). If we assume the islands containing three atoms each and counting the islands leads to an estimate of the atomic

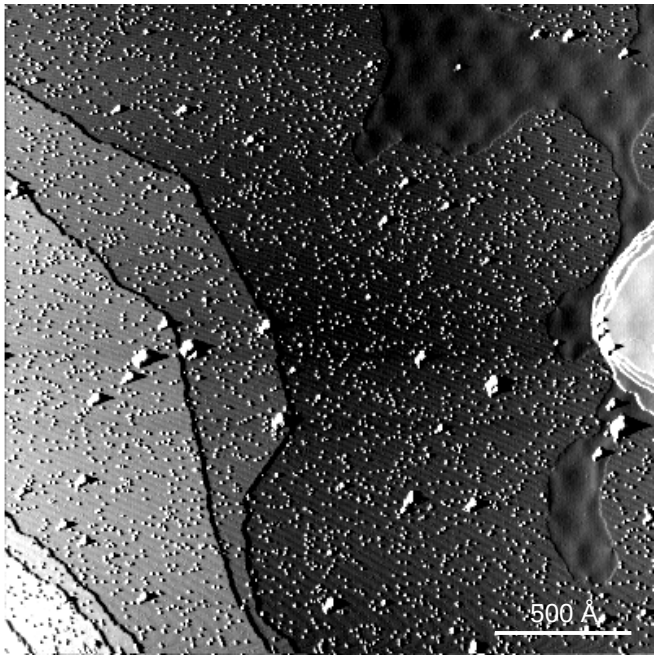

Figure 7: STM-image of $Pt_3Sn(111)$ of the mixed p(2×2) and $(\sqrt{3}\times\sqrt{3})$ R30° structure taken after annealing to 1000K, size (44Å)^2, U_t=0.9V, I_t=1.0nA. The image has been differentiated to enhance contrast. The small adatom islands mark the p(2×2) domain whereas in the lower right corner $(\sqrt{3}\times\sqrt{3})$ R30° areas with the honeycomb-network remain. The larger clusters may be due to residual contaminants, below the AES-detection-limit. From Ref. [35].

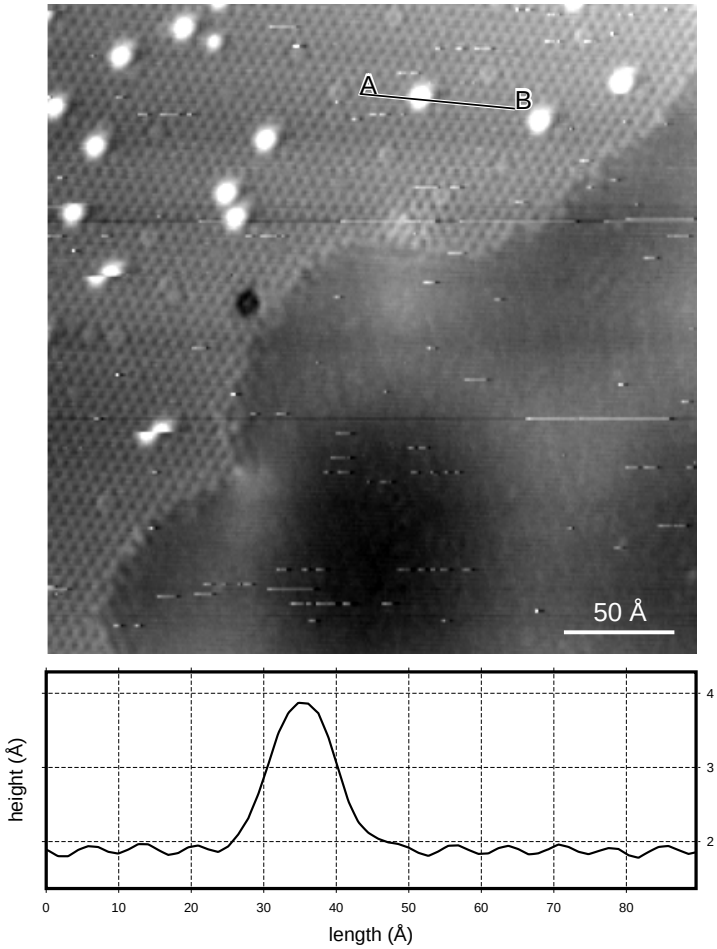

Figure 8: STM-image of the boundary region of a p(2×2) (upper left half) and a $(\sqrt{3}\times\sqrt{3})$ R30° domain on $Pt_3Sn(111)$ (lower right half, not atomically resolved), size (293Å)^2, U_t=0.9V, I_t=1.0nA. The grayscale has been restricted to the flat surface, to enhance visibility of the p(2×2) atomic structure. The height of the adatom-fe ature on the p(2×2)- region equals approx. an atomic step (section profile). Note the two adatom feat ures in the left region, which have been moved by the tip. From Ref. [35].

concentration of 1%. Quantitative LEIS data [30, 18] indicate an increase of Sn surface concentration under the annealing conditions used for the scan reported in Fig. 8. Hence we conclude that the white features are Sn islands. They result from the surplus Sn present in the $(\sqrt{3}\times\sqrt{3})$ R30°structure which is Sn rich compared to the p(2x2) structure. Obviously not all of the excess Sn atoms, ca. 8% can diffuse back into the bulk of the crystal but are stranded on the surface. The identification of the clusters as Sn is supported by recent O adsorption experiments [36]. Upon oxygen adsorption the clusters disappear and become part of the Sn-O overlayer structure formed.

The p(2x2) is the bulk truncated structure which develops under annealing via the $(\sqrt{3}\times\sqrt{3})$ R30°structure. This phase transformation was also observed

in SPA-LEED studies [18]. Extended annealing annealing times ($>$ 30 min) at 1100 K causes the p(2x2) structure to dominate completely. Higher temperature annealing causes an additional structure, defined as (2x2)', to appear. The development of the surface morphology and of the surface composition as derived from the LEIS and SPALEED study [18] is summarized in Fig. 3

3.1.2 $Pt_3Sn(001)$

The $Pt_3Sn(001)$ surface shows a more complex behavior than that of the (111). In the early studies by qualitative LEED a c(2x2) bulk termination structure was observed, but also a a "streaked" LEED pattern was reported [20, 30, 32]. The structure of the c(2x2) phase was found by quantitative LEED to correspond to a simple bulk termination model, as expected [17]. The later STM studies [27] showed that the streaked pattern originates from mesoscopic features, "pyramids" on a relatively flat surface.

In the initial reports on this surface, LEIS and qualitative LEED results for the $Pt_3Sn(100)$ surface were reported together with those for the $Pt_3Sn(111)$ one [30, 32]. The preparation of the (001) follows the identical recipe used for the (111). Ar^+ sputtering in cycles with annealing first at moderate temperatures followed by the 1000 K annealing to get a 'perfect' surface. An ordered, bulk termination "c(2x2)" phase was reported after extended annealing (see appendix for notes on the nomenclature used), but also "streaks", i.e. "extra" spots in the LEED pattern which move between the main spots when varying the electron beam energy, were reported to form after annealing at intermediate temperatures. The c(2x2) phase was analyzed by quantitative LEED [17] and a good agreement with the experimental data could be obtained by a simple bulk termination model where the uppermost layer is the "Sn-rich" plane, in agreement with the LEIS data. The LEED analysis indicated also an upward buckling (0.22 ± 0.08Å) for the tin atoms in the uppermost plane.

The STM results confirmed the LEED ones and permitted to clarify some structural elements that the analysis based on electron diffraction could not solve [27]. The STM studies were performed on samples treated in the same way (i.e. ion bombardment and annealing) as the (111) surface. Also here, the STM data were preceded and complemented by parallel AES, LEIS and LEED studies carried out in the same vacuum chamber. Evidence for Sn depletion due to preferential sputtering was reported and after the annealing at 1000 K the Pt/Sn ratio was found to be close to the bulk value by AES.

The nature of the facets observed in LEED is revealed immediately looking at the STM images (Fig. 9). The (100) surface is "decorated" with square or rectangular pyramids with a typical base width of 300 to 400 Å. The height is in the range of 40 to 50 Å. Occasionally, larger pyramids are found. The

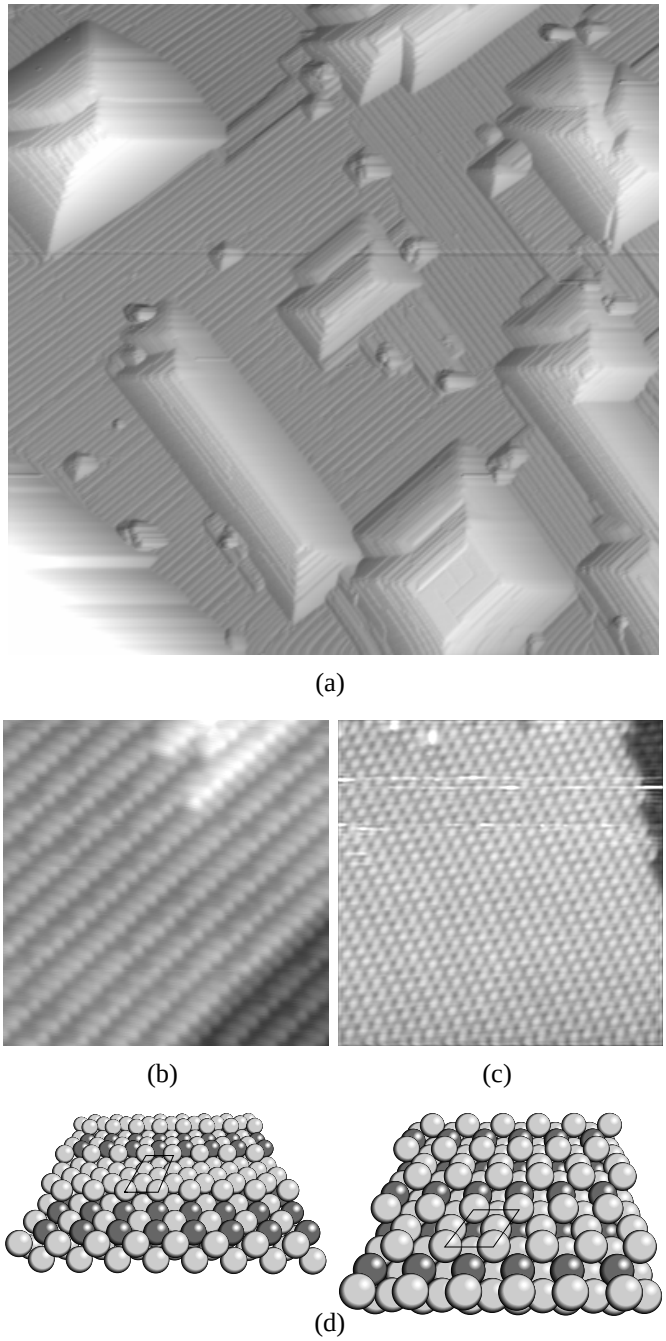

Figure 9: STM images (a-c) and marble models (d) of the $Pt_3Sn(001)$-surface after low temperature annealing. a)Overview, scan width $(1600Å)^2$, U_g=0.6V, I_t=1.0nA. b)(104)-facet on the side of a pyramid near the top. Scan width $(100Å)^2$, U_g=0.2V, I_t=1.0nA. c)(102)-facet on the side of a pyramid near the base. Scan width $(120Å)^2$, U_g=0.4V, I_t=1.0nA. d)Marble models of the (104)-facet (left panel) and the (102)-facet (right panel). For better visibility the models correspond to a chemically ordered bulk (Pt atoms light grey, Sn atoms dark grey), whereas the real pyramids are substitutionally disordered in the bulk. The unit cells seen by STM are indicated. From Ref. [27].

pyramids are sitting on a flat plane, so the structure is not 'hill and valley' as on the $Pt_3Sn(110)$ (described in the next section). A closer look to the slopes of the pyramids (see Figure) allows the identification of the facets as $\{104\}$ and $\{102\}$ respectively. The orientation of the pyramids is parallel to the [100] and [010] directions of the surface, the facets are oriented perpendicular to these directions. Marble models (Fig. 9) show these facets. The $\{102\}$ is, of course, identical to those found on (110). The difference to (110) is quite obvious, due to the fourfold symmetry, compared to the twofold symmetry of (110), the (001) surface can form $\{10n\}$ facets in two directions, which can lead to hillocks or holes with rectangular or squared shape.

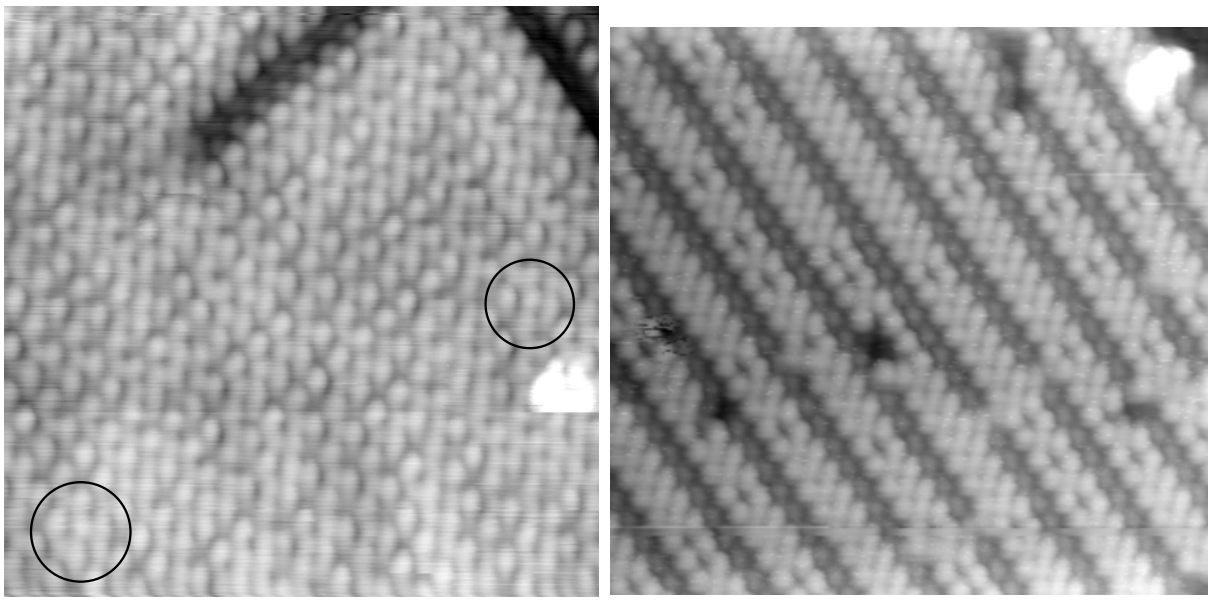

Figure 10: STM-images of a pyramid on $Pt_3Sn(001)$. Left panel) Flat top. Two unit cells with a centered atom are indicated as examples. Usually no centered atom is visible. Scan width $(80Å)^2$, U_g=0.5V, I_t=1.0nA. Right panel)Examples of 'beaded' triple rows on top of pyramids. The distance between the rows is mostly uniform but sometimes larger than shown here. Scan width $(96\times100Å)^2$, U_g=0.9V, I_t=1.0nA. From Ref. [27].

Between the pyramids the surface is not in the 'final' c(2x2) structural state, but shows a row structure parallel to the [100] and [010] directions, i.e. there are two domains of this structure (Fig. 9a). These row structures are also found on top of mostly the rectangular type pyramids (Fig. 10, right panel). The rows are made of three atomic rows, presumably Pt (see LDOS argument) with a local (100) symmetry, a square with one atom in the middle. The lateral distance of the atoms in direction of the rows is approximately 4 Å. Occasionally one of the middle atoms is missing giving the rows a 'beaded' appearance. This reconstruction seems to be an obvious way of the (001) surface to handle the Sn deficiency in the surface – quite different from the other two cases, (111) and

(110) respectively. The square pyramids tend to have a different top structure (Fig. 10, left panel). Here we observe the c(2x2) symmetry but with a surplus of Pt. As in the row structure the center of the 4 x 4 $Å^2$ square is occupied by a Pt atom, where in the annealed structure Sn has to be, and are, naturally, not visible as a protrusion with the STM.

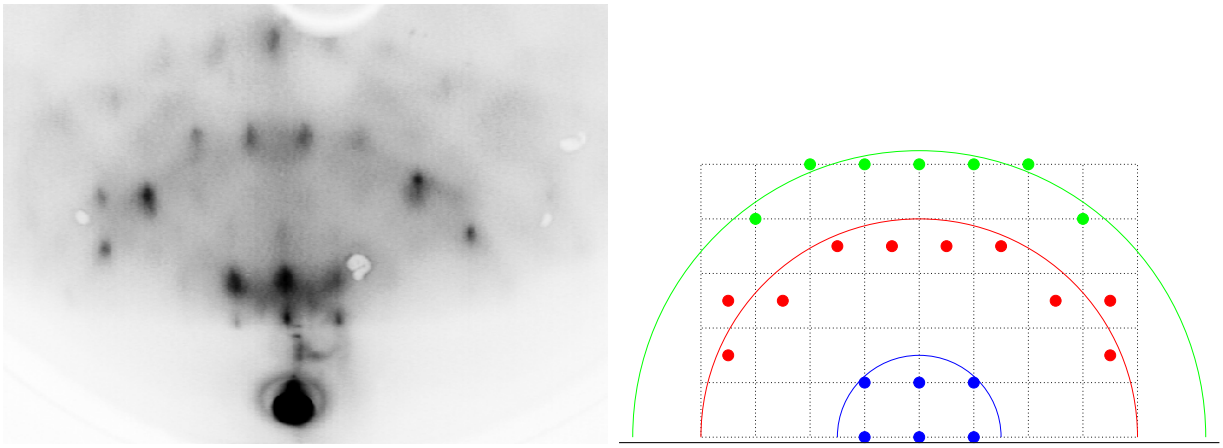

Figure 11: Experimental (left panel) and schematic (right panel) RHEED pattern of the $Pt_3Sn(001)$-surface after low temperature annealing. The main features are transmission spots lying on horizontal lines rather than Laue-circles. The Laue-circles are indicated in the schematic pattern. Electron energy is 12keV, direction of incidence is along [100]. From Ref. [27].

Before discussing more in detail the structure of the fully annealed surface we look at the RHEED results obtained from the pyramid decorated surface (Fig. 11). The RHEED pattern shows a lattice constant of the pyramids of 4.1 $\pm$ 0.3 Å in good agreement with the bulk Pt_3Sn lattice constant. However, no half order spots are observed. Such spots only appear after the 1000 K anneal indicating long range chemical order as expected for flat Pt_3Sn. We therefore conclude that the pyramids have no long range chemical order, as can be expected from the Sn deficit, i. e the pyramids are substitutionally disordered.

It is an interesting notion that the height of the pyramids corresponds to approximately 10 atomic layers or the tin depletion range found by XPD in case of the Pt(111)-Sn surface [37]. At any rate, the pyramidal form of the stress relief is the most "aesthetic" of all three surfaces under study here. A question arises with respect to the $\{102\}$ facets: why are they favored? A simple argument can be brought forward in relation to the fact that no such facets are observed on (111). The (111) surface contains no [100] rows which are the closets packed rows on (102). We find [100] rows on (110) and (001), so (102) planes intersect with these two surfaces sharing parallel atomic chains. Against $\{10n\}$ facets with odd n speaks the difference of the surface energies of Pt and Sn of 2.7 J/m^2 and 0.62 J/m^2 respectively. This difference favors facets where

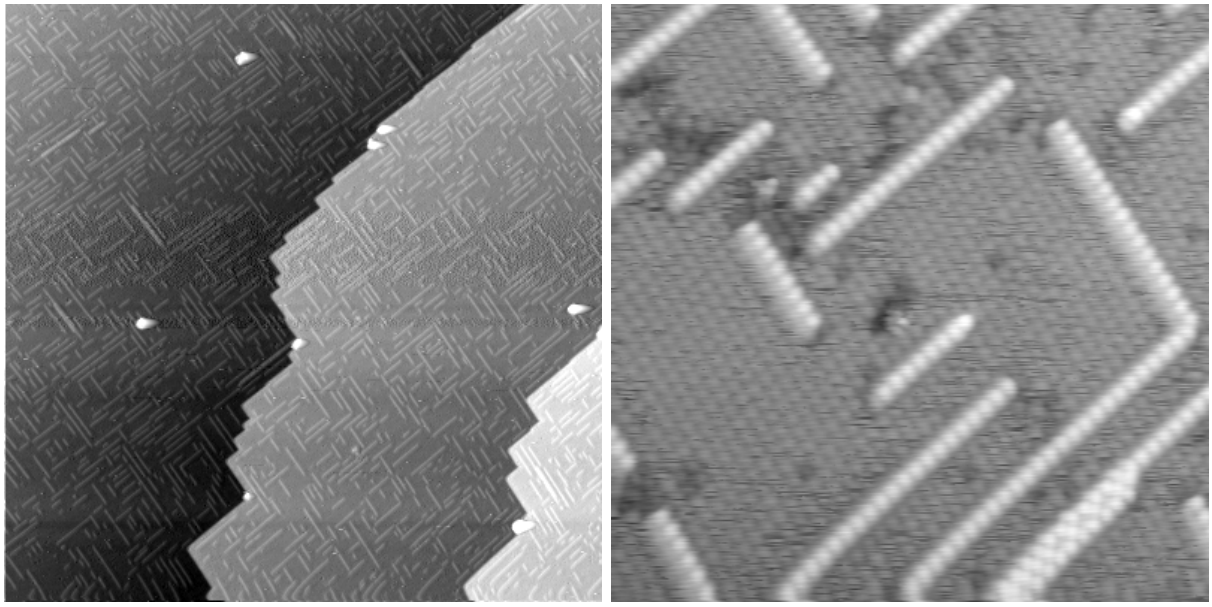

Figure 12: STM images of the $Pt_3Sn(001)$-surface after high temperature annealing (1000K). Left panel)Overview, all steps are double steps running along the [100] and [010] directions. Scan width (1700Å)^2, U_g=0.9V, I_t=1.0nA. Right panel) Close up view showing the remaining monoatomic rows and the substrate.The apparent height of the rows is 1Å. The square unit cell of the substrate shows no centered atoms, since only Pt is imaged (see text). Some defects are seen in the upper part of the image. Scan width (160Å)^2, U_g=10mV, I_t=1.0nA. From Ref. [27].

Sn rows are exposed (Fig. 9e). The $\{102\}$ facets may be preferred with respect to $\{10n\}$ with even $n > 2$, because $\{102\}$ affords the steepest slope with the smallest steps. On $\{104\}$ three row wide Pt steps occur which are less stable than terraces mixed with Sn (Fig. 9d). Note that due to the lack of chemical order within the pyramids the facets are not forced to even step height unlike the (100) and (110) surfaces of the well-annealed surface. Still, there remain open questions, for instance the balance between pyramid formation and the 'three row' reconstruction of the flat parts of (001), both structures being part of the effort to relieve the stress due to the Sn deficiency.

The fully annealed $Pt_3Sn(100)$ surface (Fig. 12) shows in STM the expected c(2x2) structure determined by LEED. All steps observed are double steps, i. e. all terraces have the identical chemical composition and structure. The pyramids tend to 'melt' away during the annealing, no Oswald type ripening effects are seen, i. e. growth of larger pyramids paid for by the small ones. Large pyramids last longer than small once, real 'big' ones are still found after extended annealing periods. Assuming that only Pt is imaged there are no protrusions in any center of the basic squares of the structure as are found on top of the pyramids, i. e. no excess Pt. What remains are single, occasionally double, atomic rows the chemical nature of which can not be determined from STM imaging. If

we carry on with the LDOS argument these rows ought to consist of Pt atoms. If we make an analogous conclusion to the (111) case the atoms could be Sn, left over from the initial sputtering and annealing effects. Adsorption experiments may shed light on this open question.

3.1.3 $Pt_3Sn(110)$

The $Pt_3Sn(110)$ surface is especially interesting in view of the fact that few studies of this orientation have been reported for intermetallic systems and also in view of the fact that many fcc metals tend to undergo surface reconstruction, e. g. Au(110) and Pt(110) form the 'missing' row (1x2) structure [38] whereas Ir(110) forms a mesoscopic hill and valley structure with (331) facets [39, 35]. The first study by qualitative LEED on the $Pt_3Sn(110)$ was reported by Haner et al. [31] . A complex behavior was reported, with a 3x1 phase forming during the initial stages annealing process, to be replaced later with a (1x2) structure (bulk truncation). The final, and apparently stable, pattern was described as "rhombic" or "quasi-hexagonal" with a periodicity in matrix notation $\begin{pmatrix} 1 & 0 \\ 1/2 & 3/2 \end{pmatrix}$. The LEIS results [20] showed that the outermost plane of this surface, as the other low index Pt_3Sn surfaces, contain tin in concentrations larger than in the bulk.

In a combined LEED, LEIS, AES and STM study the sputtering and annealing effects have been recently clarified [40]. The AES data resemble those of the(111) surface and after sputtering with 600 eV Ar ions the surface is Sn depleted. With increasing annealing temperature the Pt signal reduces and levels of at approximately 70 atomic %. The LEIS data in the same annealing range show a rather different behavior depending on the crystallographic direction too. After sputtering, the Pt concentration is approximately 50%. Annealing to 500 K causes an increase of the Pt concentration to 60% for both crystallographic directions, i. e. for scattering along $[\bar{1}10]$ and $[00\bar{1}]$ respectively. In the temperature range between 600 K and 900 K the surface becomes Sn rich, before, at 1000 K, an equilibration of the surface concentration at approximately 50 and 60% is reached for the two respective crystallographic directions. We can assume that at most the two outermost layers contribute to the Pt LEIS signal [41]. Therefore, when scattering along $[\bar{1}10]$ two layers contribute to the Pt signal, 50% from the topmost layer and about 10% from the second layer. The lower signal from the second layer is due to the remaining depletion in the second layer (AES) and due to the enhanced neutralization of the He ions used for scattering from the second layer. For scattering along $[00\bar{1}]$ the signal of the second layer is reduced by additional blocking. The LEED pattern for intermediate annealing contains (1x1), (2x1) and facet beams. The facet beams

show the proper ‘wandering’ when changing the electron beam energy. Sometimes these spots smear out into streaky features as reported earlier. The fully annealed surface is clearly (1x2).

The structure of the surface and the identification of the “extra” beams observed in LEED is straightforward when looking at the STM topographs (Fig. 13). What do we see? The main features are steps and/or facets running perpendicular to the $[\bar{1}10]$ surface direction. There are ‘up’ and ‘down’ regions, that is the surface has a mesoscopic hill and valley structure (Fig. 13 b). From the height scan as in Fig. 13 b the slope of the facets can be determined as $\pm$ 18.4° with respect to the (110) plane. This angle is the crystallographic angle to (102) planes, i. e. the facets observed are $\{102\}$ with a distance of 1.5 $a_0/\sqrt{2} = 4.24$

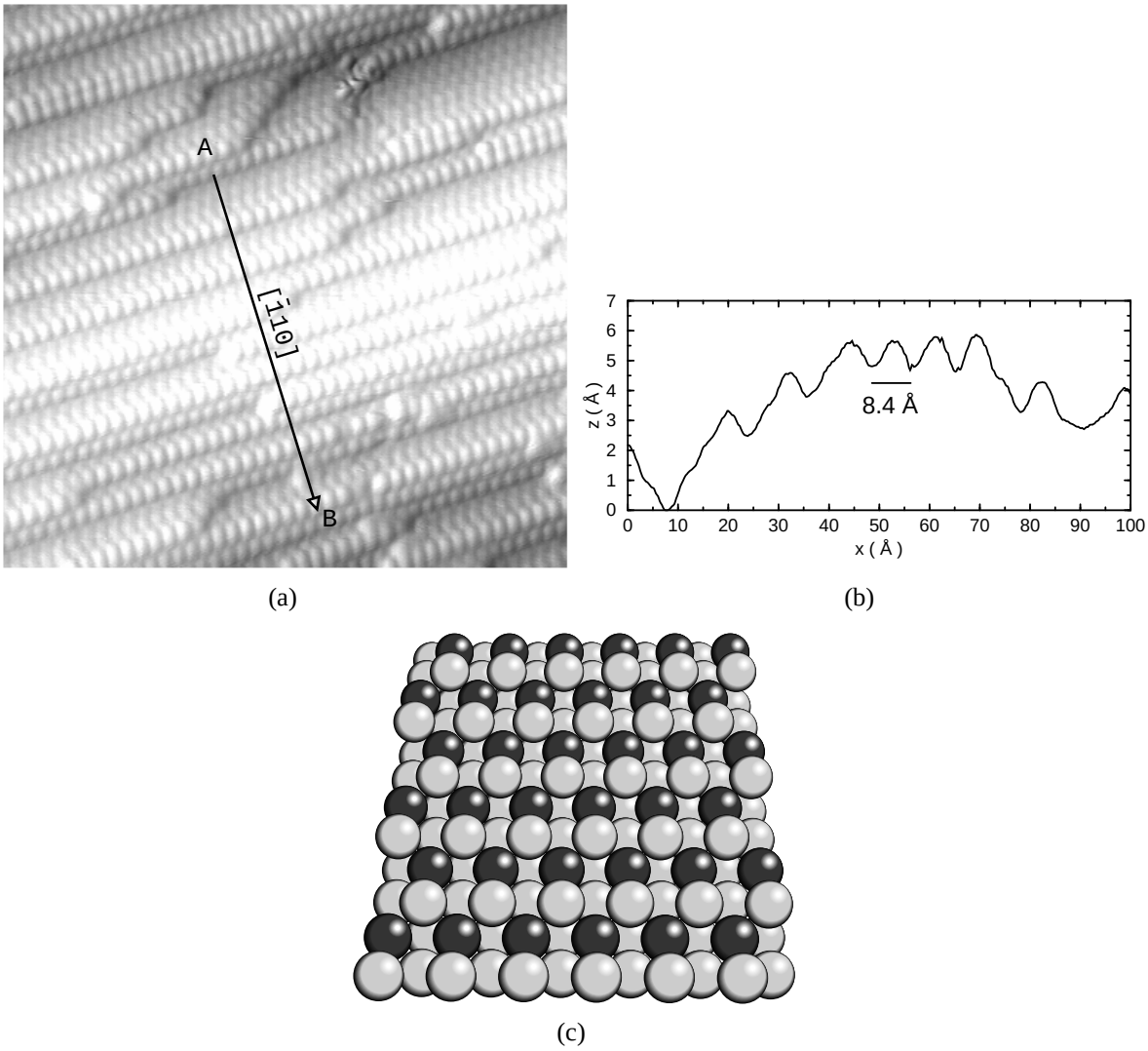

(a) (b)

(c)

Figure 13: STM image of the $\{102\}$ facets on the $Pt_3Sn(110)$ surface after anneal to 715 K, 154 Å, -0.15 V, 2.5 nA (a), height scan between A and B along $[\bar{1}10]$ (b) and sphere model of a non-bulktruncated $\{102\}$ facet, that is in accordance with the data. From Ref. [40].

Å between adjacent [00$\bar{1}$] rows. The shortest possible period of the facets can be 8.5 Å which is e. g. observed in Fig. 13 b. Based on these findings we can construct a marble model of the faceted surface (Fig. 13 c).

The hill and valley structure must be the result of the tensile stress induced in the (110) surface due to the depletion of Sn during sputtering. The stress relief is anisotropic with ripples perpendicular to the [00$\bar{1}$] direction thus creating $\{102\}$ facets. The orientation of these facets is in accordance with the LEED observations. As a consequence of the choice of these facets the [001] rows exposed on the facets are all monoatomic, i. e. either Pt or Sn. The exposure of the Sn atoms of these rows on then facets is the most plausible explanation for the Sn surplus observed by LEIS at the intermediate annealing stage. The corrugation of the hill and valley structure reaches approximately 4 to 5 atomic layers or about 1/3 of the Sn depleted region.

As in the case of the (110) surface, higher temperature annealing causes the growth of larger terraces and the gradual disappearance of the $\{102\}$ facets (Fig. 14). The terraces are bordered by steps of 2.8 Å in height or multiples thereof, i. e. composed of double steps (Fig. 14 c and d). Double steps are the consequence of the surface termination by only one type (as on $Pt_3Sn(100)$, Fig. 12, left panel). The slope of the steps in [00-1] direction is $\pm 18.4°$ again. So we find here $\{102\}$ facets as in case of the intermediate annealing state in the hill and valley structure. The slope of the double steps in [$\bar{1}$10] direction is 22.5° which is smaller than the expected 35° with respect to the (110) planes for $\{111\}$ facets. The $\{111\}$ facets are expected from the marble model constructed for the step structures observed (Fig. 14 e). We suspect the 35° are too large an angle for the STM tip to follow. Additionally there is always the possibility of electronic smoothing due to the Smoluchowski effect. Further details resolved with smaller scanning areas of the step structures (Fig. 15) support the identification of the step directions and the interpretation using the marble model of Fig. 14 e. The atomic corrugation of a fourfold step is, for example, clearly resolved in Fig. 15 b. Since we never observe 'uneven' steps we have an additional strong argument for the termination of the crystal. Final support for the mixed termination comes from high resolution STM images with different bias voltages (Fig. 16 a, b). Knowing the orientation from the crystal and having the STM piezos calibrated it is obvious that the apparent surface lattice constant is larger along [$\bar{1}$10] directions than along [00$\bar{1}$] directions. As in case of the (111) and (100) surfaces we can safely assume that the bright spots in the STM images are Pt atoms. The contrast of these spots is also hardly dependent of the bias voltage applied between tip and sample. At negative bias, i. e. when probing the filled states, the Pt atoms appear brighter or larger than at positive bias. These findings are consistent with the interpretation of the STM images with

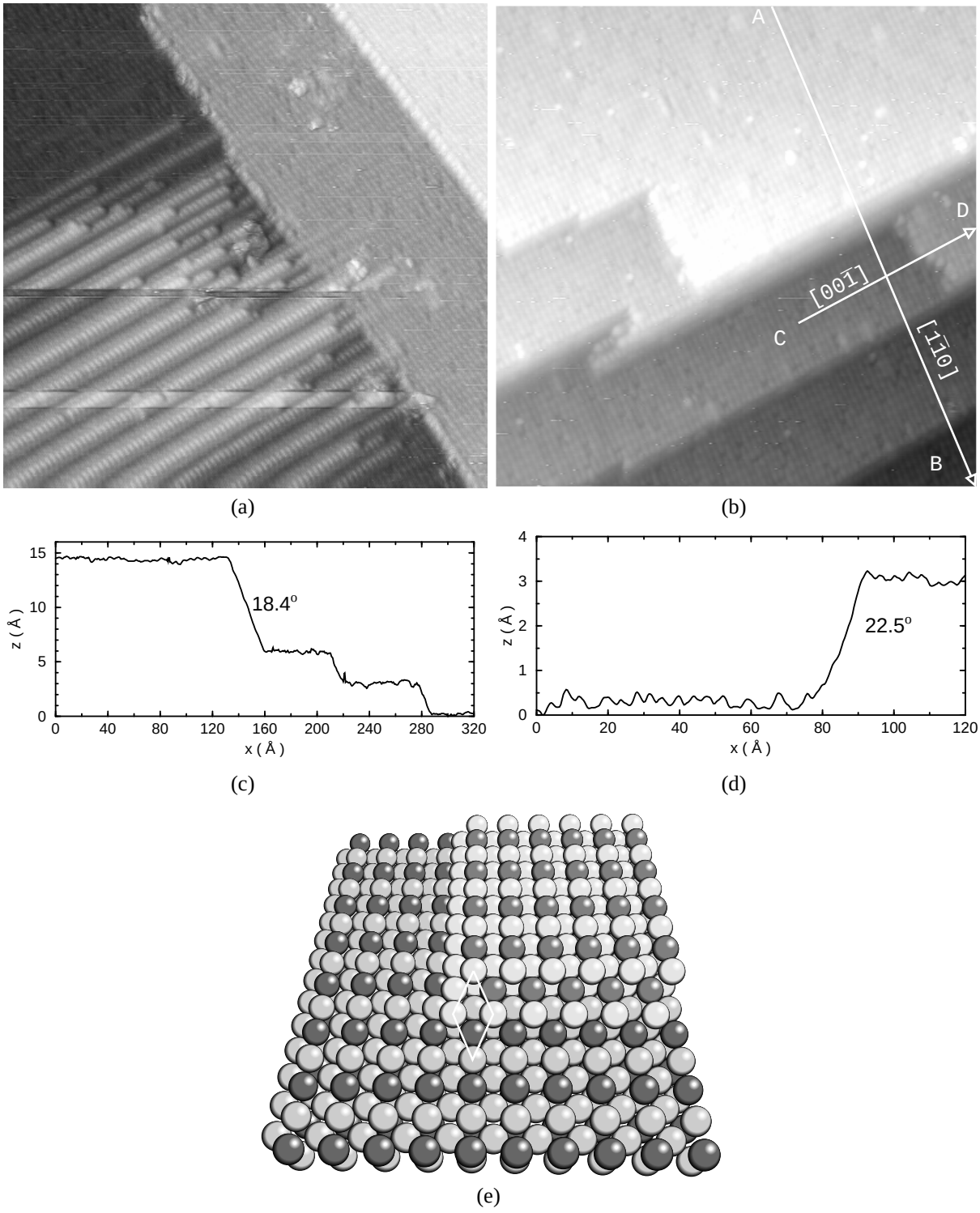

Figure 14: STM images of coexisting faceted structures and flat terraces on the $Pt_3Sn(110)$ surface, T_{anneal}=920 K, 300 Å, 0.4 V, 0.8 nA (a) flat surface T_{anneal}=920 K, 300 Å, 0.5 V, 0.8 nA (b) with height scan between A and B along $[\bar{1}10]$ (c) and height scan between C and D along $[00\bar{1}]$ (d). Sphere model of double steps (e). Note that the minifacets along the $[\bar{1}10]$ double steps are $\{111\}$ oriented and the multiple minifacets along the $[00\bar{1}]$ steps are $\{102\}$ oriented as found on the real surface. At the $\{102\}$ the structure model deviates from the bulktermination, in accordance with the data. From Ref. [40].

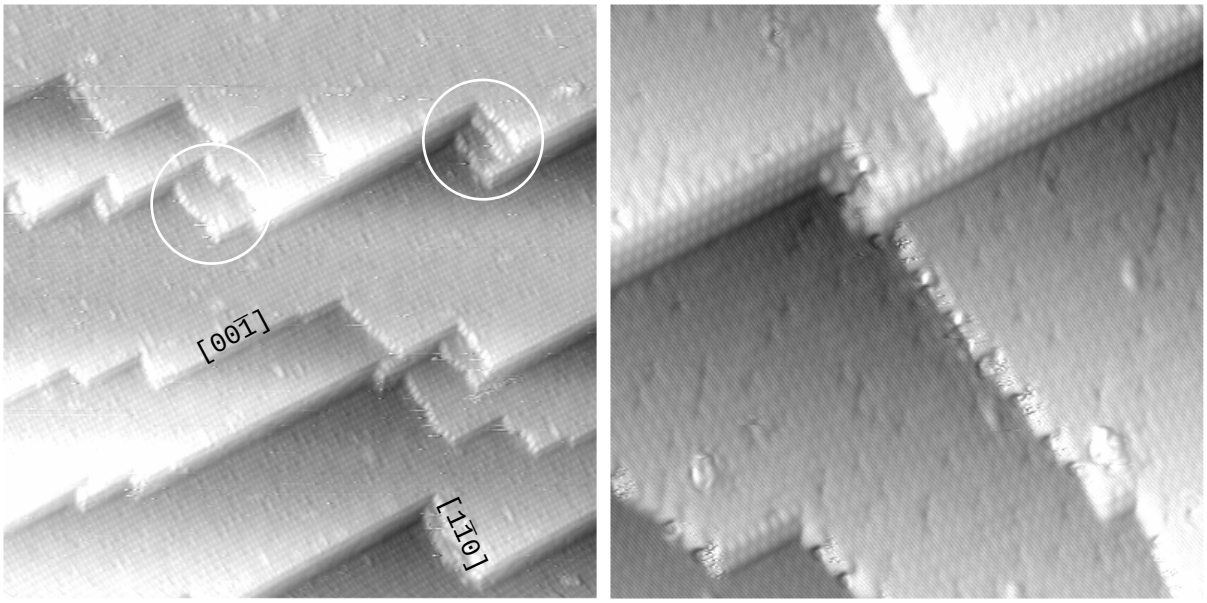

(a) (b)

Figure 15: STM images of merging double steps on the $Pt_3Sn(110)$ surface, 500 Å, 0.45 V, 0.8 nA (a) and 200 Å, 0.40 V, 0.8 nA (b). The $[00\bar{1}]$ steps form double, fourfold and sixfold steps whereas the $[\bar{1}10]$ steps are predominantly double. From Ref. [40].

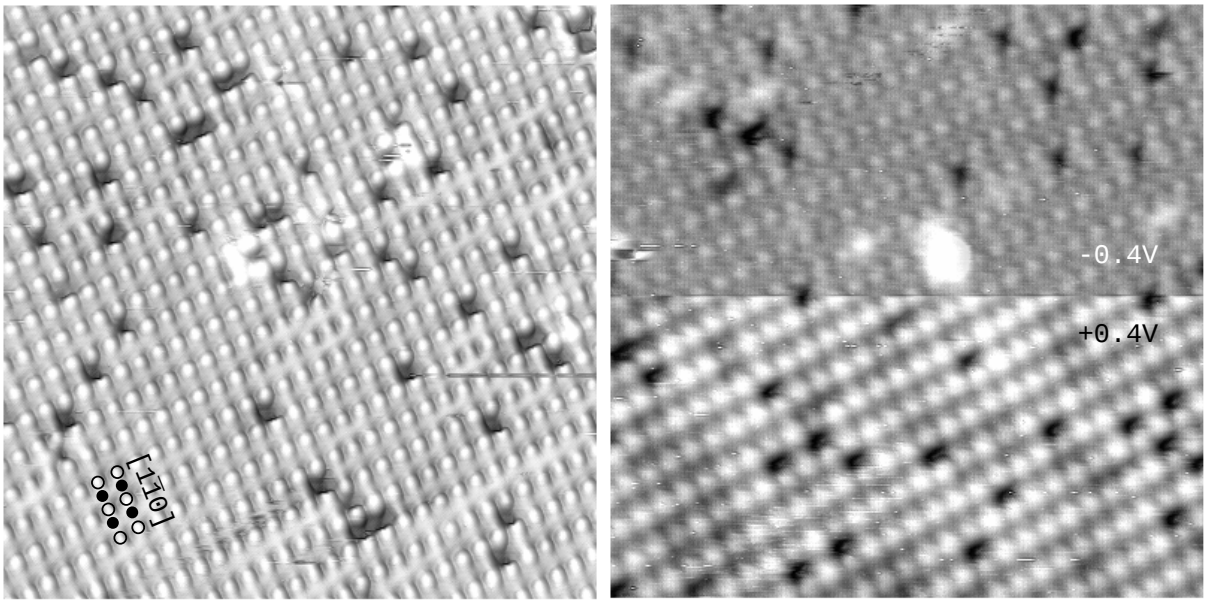

(a) (b)

Figure 16: STM images of the $Pt_3Sn(110)$ surface, a) 120 Å, 0.5 V, 0.8 nA. Pt atoms are visible as protrusions (open circles), Sn atoms are invisible (filled circles). b) 100 Å, +0.4 V (lower part) -0.4 V (upper part), 0.8 nA. The Pt atoms appear bigger when measuring the empty states (lower part). The contrast is higher when the filled states are measured (upper part). The big bump in the middle is presumably a contamination. From Ref. [40].

help of the LDOS data. In turn, this means that the holes are real Sn vacancies rather than an electronic tip effect. It is, furthermore, interesting to note that in case of the (111) surface we find a surplus of Sn on the well annealed surface, whereas the (110) tends to be depleted of Sn.

3.2 Surface alloys obtained depositing tin on platinum surfaces

The term "surface alloy" is somewhat generic and may refer to a variety of different systems. Here, we apply it to those systems where ultra-thin metal layers (i.e. a few atomic layers thick) are deposited on a bulk metal surface and where the system is subsequently annealed in vacuum in order to obtain alloying in a surface region a few atoms thick. In these conditions it is possible to obtain *single* atomic layer binary phases, or *multilayer* surface alloy phases (also termed "epitaxial alloys" (for a general discussion of these surface alloys, see [5]. Relatively to the subject of the present paper, two Pt-Sn systems have been studied Sn-Pt(111) and Sn-Pt(100). The behavior and the structural properties of these systems will be discussed in detail in the following.

3.2.1 Sn-Pt(111)

The first study of Sn deposition on Pt(111) was reported by Paffet and Windham in 1989 [42] and a subsequent one on the same system was published by Campbell in 1990 [1]. In both studies, two LEED patterns were observed after annealing: a 2x2 and a $(\sqrt{3}\times\sqrt{3})$ R30°. Both superstructures were interpreted in terms of incorporation of the tin layer in the first platinum layer, but only a qualitative examination of the LEED pattern was performed. Subsequently the results of low energy alkali ion scattering spectroscopy ALISS [43, 21] could be quantitatively interpreted as due to ordered, single atomic layer surface alloys. The ion scattering results have been confirmed and expanded by a quantitative LEED study [34]. The atomic structure of both phases corresponds exactly to that of the topmost layer of the phases with the same periodicity observed on the on Pt_3Sn(111). The LEED and ALISS results for the Sn/Pt(111) system were confirmed by a recent STM study reported by Batzill et al. [44]. Even though atomic resolution was not attained in this study (only the surface unit mesh could be observed), the results are closely comparable to the atomically resolved ones obtained on the Pt_3Sn(111) surface [35].

The formation of multilayer surface alloys has also been investigated in the Sn-Pt(111) system, where Galeotti et al. [37] reported the formation of ordered, epitaxial alloyed Pt-Sn phases. The deposition of amounts of Sn up to 5 monolayers (ML) at room temperature led to disordered or anyway non-epitaxial tin films. Annealing the deposited films led to interdiffusion and to the formation of various alloy phases (Fig. 17). Alloying was detectable in XPS from the

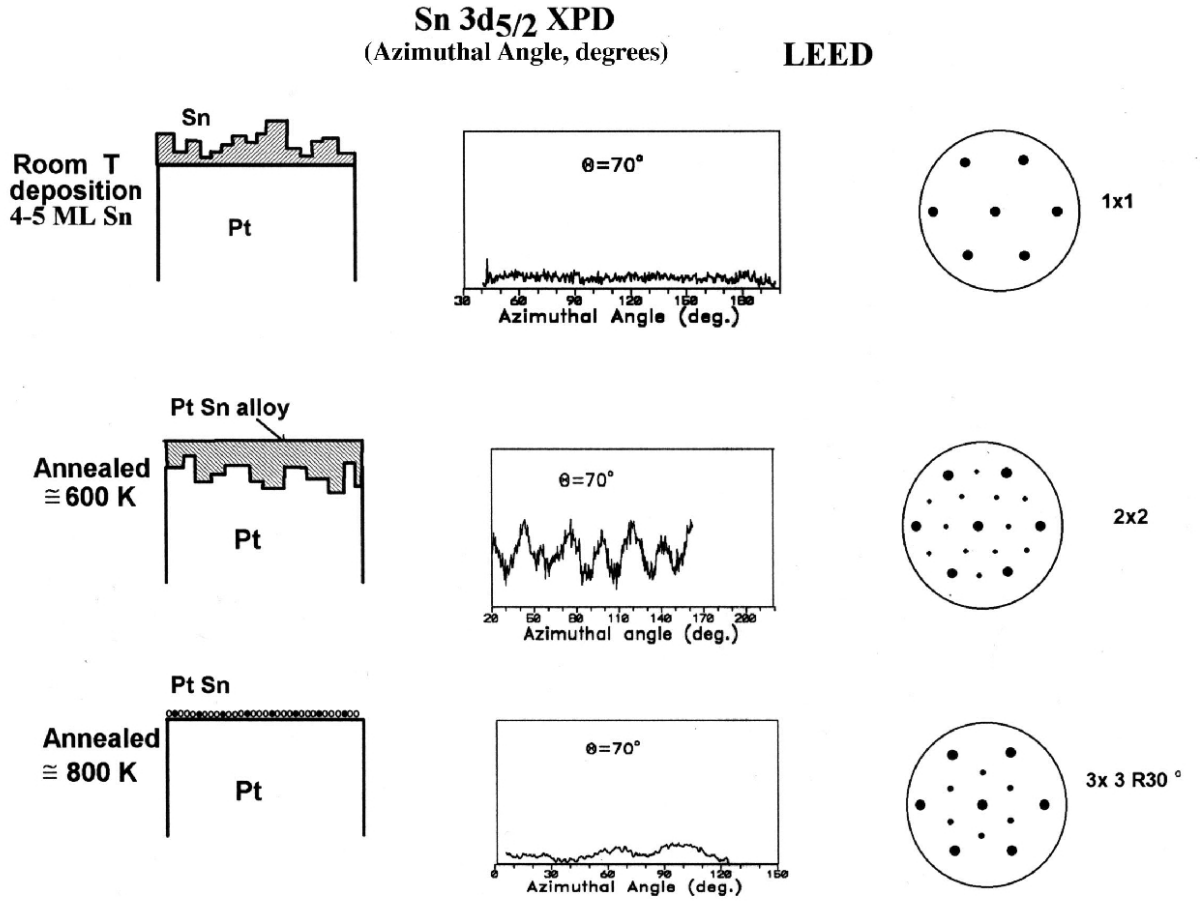

Figure 17: Main results obtained by combined LEED and XPD measurements on the Sn/Pt(111) system. The left row is a schematic representation of the surface structure. The center row shows the XPD results for the Sn$3d_{5/2}$ peak. The absence of oscillations in the pattern indicates either a disordered surface ("as deposited") or a single atomic layer (after high temperature annealing) where "forward scattering" effects cannot play a role. The right row shows the LEED results corresponding to the structural models described in the text. From [37].

shift of the Sn core level peaks 0.3 eV with respect to the "as deposited" Sn film. The formation of multilayer surface alloys could be clearly evidenced by XPD after depositing amounts of tin in the range of 3-5 MLs and annealing at temperatures ranging from 400 to 600 K. In LEED, this phase showed a (2x2) translational symmetry. Because of the forward focussing effect, the observation of strong oscillations in the XPD curves for Sn implies that in this phase a significant fraction of tin atoms are located below the surface. A further result that can be derived from the XPD data is that the Sn atoms are located in the same local environment of the Pt atoms. Furthermore, the similarity of the XPD results indicates that the near-surface structure of the Sn/Pt(100) system is the same as that of Pt_3Sn(111) sample. The identity of the two phases is confirmed by calculations performed for a bulk truncation model of the Pt_3Sn(111) surface. Since the LEED results clearly show long range ordering, it is possible

to arrive to a univocal model for the (2x2) phase that involves the formation on the surface of an ordered alloy multilayer of the same structure as that of the bulk, ordered $Pt_3Sn(111)$ intermetallic compound. The difference in the lattice parameter in Pt_3Sn and pure Pt is small and the unit mesh for the ideal bulk truncated structure of the (111) plane of the alloy can be described as (2x2), indexing the diffraction spots with respect to the Pt(111) surface.

After annealing the (2x2) multilayer surface alloy at 1000 K for several minutes, a $(\sqrt{3} \times \sqrt{3})$ R30°LEED pattern was observed again. In these conditions, the XPD azimuthal curves for the Sn 3d are flat, as those for the $(\sqrt{3}\times\sqrt{3})$ R30°phase obtained starting from Sn coverages of the order of 1 ML (Fig. 17). This result indicates that for extended annealing a '2-dimensional' alloy is formed again and that at this temperature tin atoms diffuse from the surface into the bulk to a depth that cannot be probed by the photoelectrons. This transformation is schematically described in Fig. 17, together with an illustration of the significant LEED and XPD results.

The well characterized and stable surface phases observed on the Sn-Pt(111) have provided researchers in the chemisorption and catalysis field with a substrate of great interest for studying the properties of bimetallic interfaces. Simple "probe" gases such as CO have been studied after adsorption on this system [45] as well as a variety of organic molecules such as acetylene [46], cyclohexane and benzene [47, 48], butane and isobutane [49], methanol, ethanol and water [50]. Several surface reactions of the above gases were also studied.

3.2.2 Sn-Pt(100)

The first study on this system was published by Paffett and Whindham [42] together with the results for the Sn/Pt(111). After deposition of an amount of Sn of ca. 3 ML and subsequent annealing, two periodicities were observed in LEED: a c(2x2) and a $(3\sqrt{2} \times \sqrt{2})$ R45°. These surfaces were studied from a quantitative structural viewpoint by Li and Koel [23] by ALISS. The experimental setup and the methods used was similar to that used for the Sn/Pt(111) system. Here, the clean Pt substrate surface starts reconstructed, showing in lead the well known "streaks" which have been indexed in terms of a (5x20) periodicity. The formation of a c(2x2) phase was observed after depositing 0.5 ML of tin and annealing in the range 400-700 K. In this range the ALISS polar angle scan was interpreted in terms of an overlayer of tin atoms, i.e. not a surface alloy. At higher temperatures (T>ca. 750 K) considerable structural changes were observed. In this case, the ALISS results clearly indicated the formation of a substitutional Pt-Sn alloy of the same structure as the bulk termination of $Pt_3Sn(100)$. In this phase, buckling of the Sn atoms was foind to be very small (0.17-0.22 A). The data do indicate the presence of this substitutional alloy in

the topmost surface layer, however, evidence was observed for the presence of tin in the deeper layers.

The alloyed c(2x2)-Sn structure on Pt(100) was found to be unstable and to quickly transform into the $(3\sqrt{2}\times\sqrt{2})$ R45°phase which was found to be stable up to annealing temperatures of 1000 K. It was not possible to propose a complete model for this phase, however the ALISS results remained very similar to those for the c(2x2) phase. It was therefore suggested that the the local structure of the $(3\sqrt{2}\times\sqrt{2})$ R45°is the same as that of the c(2x2). Indeed the c(2x2) periodicity can also be written in an equivalent manner as $(\sqrt{2}\times\sqrt{2})$ R45°. The "extra" $3\sqrt{2}$ periodicity observed for the Sn-Pt(100) surface can be due to a specific step arrangement or periodic domains of pure Sn atoms every three lattice spacing along the [100] azimuth.It appears that the formation of the $(3\sqrt{2}\times\sqrt{2})$ R45°is accompanied by the disappearance of tin atoms from the subsurface region.

No STM results have been reported so far for the Sn-Pt(100) system so it is not possible at present to know if the metastable pyramids observed on the $Pt_3Sn(100)$ surface are present also on the surface alloy. Chemisorption and catalysis studies are also lacking for the Sn-Pt(100) system which has not been found as attractive as the Sn-Pt(111) because of the lack of stability of the c(2x2) phase and for the difficulty of quantitatively characterizing the $(3\sqrt{2}\times\sqrt{2})$ R45°one.

4. DISCUSSION

Among ordered bimetallic systems, the Pt-Sn one can be considered at present as the most in-depth studied not only for its surface structural properties, but also for its reactivity and catalytic properties. A comparable detailed knowledge exists only for a few other cases, among platinum alloys we can cite the Ni-Pt and Co-Pt systems, examined for their catalytic properties and the Pt-Ti system studied for their electrocatalytic properties [5]. Sparse data relative to the surface properties of several other Pt alloys exist (e.g. Fe_3Pt and Cu_3Pt - [3] and Pt_3Mn [51]. All these data available pertain to fcc phases either random substitutional or ordered compounds. Data exist also for other cubic ordered alloys which are isostructural with the Pt3Sn compound, e.g. Ni_3Al [52, 53] and Au_3Pd [28] and finally the Au-Cu system, which has been object of interest as the "prototypical" $L1_2$ or $Pm3m$ ordered system in the Cu_3Au composition [54, 55].

If we consider also the availability of theoretical studies on the surface segregation and equilibration phenomena [7] the Pt-Sn system can be seen as the most thoroughly characterized in a whole class of alloys, that of "ordering" al-

loys, i.e. alloys which tend tend to form ordered bulk intermetallic compounds with a highly negative enthalpy of formation. We'll see in the following that the surface structural behavior of alloys in this class appears to be similar for the known cases, but that the Pt-Sn system shows a complex series of surface reconstructions not observed on other alloy systems.

Regarding the high bonding energy of some Pt alloys system we note that already in the 60s Leo Brewer [10] had put forward a simple model (sometimes referred to as the "Engel-Brewer model") which could be used for a qualitative prediction of the strength of the intermetallic bond. The Brewer model predicted charge transfer between different metallic species in reason of the different electronegativity. It is well known how ionic compounds (e.g. NaCl) form by the reaction of elements of the far left and far right row of the periodic table. Something analogous takes place with the transition elements, with the elements of the IVB and VB rows forming highly exothermic alloys with elements of the VIIIB row (e.g. Pt-Ti, Pt-Zr, etc). Conversely, alloys of elements of the same row tend to have small enthalpy of formation and therefore to form random solid solutions or compounds which have a low temperature of order-disorder transition. A classic example here is the Cu_3Au alloy which has a transition temperature of 663 K. Indeed this transition has been the main motive of interest which led to the first LEED surface studies on a bimetallic system to be performed on this compound, which can be by now considered a "classic" [56, 57, 54, 58, 59, 55, 60]. On the contrary Pt_3Ti, for instance, is an ordered compound in the whole range of temperatures below the melting point and has a highly negative enthalpy of formation of -19.5 Kcal/mole [61].

In recent times, the electronic structure of transition metal alloys has been studied with more advanced methods. The basic Engel-Brewer model has been confirmed when the intermetallic bond has been correlated to a shift in the overlayer local d-electron band and a simultaneous dip in the noble metal (e.g. Pt) d-electron local density of states (LDOS) at the Fermi level. These models, however, do not directly apply to the platinum-tin system since tin is not a transition element. However, tin is an electropositive element and so, according to the Engel Brewer model, the properties of Pt-Sn alloys in terms of enthalpy of formation could be expected to be comparable to those of the strongly exothermic alloys of platinum. It has been found that in Pt- non transition metal alloys, the same dip in the LDOS observed in Pt-transition metal allos is caused by the hybridization of d-electrons with the p-electron band [62]. According to Pick [63] the electronic structure of noble metal/ non transition metal alloys is therefore very similar to that of noble metal/transition metal alloys. This electronic structure leads to a series of consequences, not the least interesting one the change in reactivity towards adsorbates, a subject which will not reviewed

here for lack of space, but which has been studied in detail for the Pt-Sn system.

4.1 Surface atomic structure of bulk Pt_3Sn alloys

In most - but by no means all - studies of binary alloy systems reported so far, qualitative LEED data indicate that the surface unit mesh corresponds to what expected from truncation of the bulk lattice [5]. The observation of the "expected" pattern in LEED in itself is no proof that the surface atomic structure is actually the bulk truncation one. Furthermore, in the case of ordered intermetallic compounds, the 'bulk termination' model is not normally univocal since the planes stacked along a specific crystallographic direction do not necessarily have all the same composition. In the case of fcc Cu_3Au ($L1_2$) ordered compounds (Fig. 1) all the crystallographic directions, except the $\langle 111 \rangle$ have an ...ABAB... stacking with – for instance in the case of Pt_3Sn – a plane of pure Pt alternating to a plane of composition PtSn. Both terminations correspond to 'bulk truncation'; and in both cases the composition of the outermost plane is different from the average one of the bulk.

The experimental observations by LEIS of a number of bimetallic systems have shown that in the preferred termination may be either "mixed" or "pure" depending on the chemical species present. Quantitative surface crystallographic methods (especially dynamic LEED) have confirmed the LEIS results. The cases where the atomic structure of the topmost layer corresponds to that of a "mixed" bulk crystallographic plane For the $L1_2$ phase (fcc, Cu_3Au type) has been reported, among other cases, for instance for $Cu_3Au(100)$ ([56, 57, 54, 58, 59, 55, 60] and $Ni_3Al(100)$ [52, 53] systems which have the same structure and termination as the $Pt_3Sn(100)$ [17, 27]. In all these cases, obviously, the presence of different degrees of outward relaxation ("buckling") for the different chemical species present has been reported.

Other bulk isostructural compounds show a "pure" termination instead of a mixed one. This behavior was observed in the case of the $Pt_3Ti(100)$ surface, a result obtained independently from LEIS [64] and LEED data [65]. Also the $Pt_3Ti(111)$ surface was found to be enriched in Pt [64, 66]. This behavior, which is in sharp contrast with that of the isostructural Pt_3Sn case, may be related to the difference in the relative sizes of the atomic species involved (Ti and Sn). It may also be worth to consider the possibility that it could be attributed to differences in bulk composition. The Pt_3Ti sample used in the crystallographic studies [65] had a nominal 3:1 Pt /Ti atomic ratio, but there are elements suggesting that a sequel of successive treatments of ion bombardment and annealing led to a depletion in titanium of the selvedge region [67]. The irreversible depletion in the light element in the surface of a bulk alloy as the effect of extended ion bombardment was reported for NiAl(100) [68],

Table 1: Summary of the structures observed on Pt_3Sn surfaces after annealing at moderate and high temperature

	600 K - 800 K	1000 K -1100 K
(111)	$(\sqrt{3}\times\sqrt{3})$ R30°(Pt_2Sn), mesoscopic subsurface dislocation network	p(2×2) , adatom islands
(001)	multiple row structure, pyramids bordered by {102} and {104} facets	c(2×2) , double steps, single atomic ad rows
(110)	hill-and-valley-like structure with {102} facets	(2×1) , double steps, holes at Sn positions

$Pt_{80}Fe_{20}$(111) [69] and $Pt_{80}Co_{20}$(100) [70]. Theoretical calculations based on the broken bond model [71] indicate that Pt segregation in Pt_3Ti is expected for an excess of platinum in the bulk with respect to the 3:1 stoichiometric ratio. Hence, the actual bulk composition, as opposed to the nominal one, may have an effect on the surface composition and structure of an alloy. For the case of Pt_3Sn, there are elements indicating that the "as prepared" Pt_3Sn single crystal samples used in the surface studies reported here were slightly "Sn-rich" in comparison to the nominal composition, for instance the observation of excess tin on the topmost layer of the Pt_3Sn(111) surface which appeared as "white spots" in the STM scans [35, 40]. The effect of the several cycles of ion bombardment and annealing may have progressively reduced this excess of tin. Although these phenomena are an indication of a complex behavior of the Pt_3Sn system (and in general of bimetallic alloy materials), their effect on the topmost surface composition should not be overestimated. Indeed in the case of systems obtained by depositing tin on pure platinum substrates, the excess of platinum is an obvious condition. Nevertheless, two-dimensional surface phases containing tin have been observed (as it will be discussed more in detail later) indicating that there are chemical factors which lead to stabilize tin in the outermost layer independently of the bulk composition. These factors, conversely, appear to destabilize the presence in the topmost layer of such elements as Ti, Co, and Ni. Summarizing, the "mixed" termination is by no means to be taken for granted in all Pt-M system. It does, however, seem to be the general case for the Pt-Sn system.

Although the observation of bulk truncation phases in the Pt_3Sn(hkl) case is not surprising, the wealth and complexity of the reconstructions observed is remarkable, as well as the interplay of the factors which lead to the transitions observed among them. A list of the phases observed for the Pt_3Sn system is provided in Table 1 . Surface reconstruction, that is a surface mesh that is not the same as the bulk mesh along the surface plane, has been observed also for other alloys. The random substitutional Pt alloys $Pt_{80}Co_{20}$ (001) [72], and $Pt_{50}Ni_{50}$ (100) [16] show a "pseudo-hexagonal" reconstruction similar (but not identical)

to the one observed on pure platinum surfaces and by some other pure transition metals [73]. In both cases the composition of the outermost layer appears to be pure platinum. Conversely, small amounts of deposited metals (e.g. zirconium on Pt(100) [67]) destabilize the Pt reconstruction, reverting the surface to the "expected" 1x1 structure.

Reconstructions similar to the ones observed on the Pt-Sn system have been observed in some other cases of binary alloys. For instance for Cu-Al(111) [74] the quantitative LEED analysis [75, 76] showed that the topmost layer is a mixed plane of the same structure of the reconstructed $Pt_3Sn(111)$ surface. Also a $(\sqrt{3}\times\sqrt{3})$ R30°reconstruction has been observed for the (111) surface of the random substitutional Al-6.5at% Li alloy, [77] (Quantitative crystallographic data not available). Nothing comparable to the "pyramidal" structures observed by STM on the $Pt_3Sn(100)$ system has been reported so far for other alloy systems.

The theoretical interpretation of these results is still in progress but the main elements leading to stabilize some reconstructions seem to be well established. Foiles [78] used the EAM method to study the stability of surface ordered phases low index surfaces of dilute Cu-Au (111) alloys. The calculations indicate a domain of Au bulk concentrations (from ca. 0.001 at% to 5 at%) that produce surface segregation and the formation of stable p(2x2) and $(\sqrt{3}\times\sqrt{3})$ R30°surface alloys respectively on the (100) and (111) planes. The theory in this case seems to quantify intuitive considerations based on two facts: i) that the Au-Cu bond is energetically favorable and ii) that Au has a larger radius than copper. These two conditions lead to different tendencies; the first to have Au stay in the bulk to maximize the number of Cu neighbors, the second to squeeze Au atoms from the bulk to the surface where outward relaxation can be energetically favorable. The interplay of the two tendencies leads to an intermediate condition where Au atoms form a single layer phase where they increase the intermetallic bond distance by relaxing outwards. These consideration can help to understand why this kind of reconstruction occurs for dilute, random substitutional alloys.

The case of Pt-Sn is more complex and whenever the concentration of the minority metal in the bulk is not negligible, and especially in the case of ordered intermetallic compounds, it is necessary to consider that heterogenous bonds occur in the interaction of the first layer with the underlying one. Consider the $Pt_3Sn(111)$ case, here the highest packing periodicity in the topmost plane, the $(\sqrt{3}\times\sqrt{3})$ R30°, see the structure shown in Fig. 4, leads necessarily to a number of Sn-Sn nearest neighbors between the topmost and of the second layer (assuming that the latter would maintain the expected bulk structure). Since Sn-Sn bonds are less energetically favorable than Sn-Pt ones, the forma-

tion of the $(\sqrt{3}\times\sqrt{3})$ R30°phase should be unfavorable and indeed it is observed on Pt_3Sn only when the substrate is strongly depleted in tin as the result of a ion bombardment [33]. As a rule of thumb, the segregating species is the material with the lower melting point or cohesion. Obviously, the surface is much more driven out of the equilibrium situation when the preferentially sputtered species is identical with the segregating one, as in Pt-Sn alloys. Then, the segregation can take place only after the composition has been restored, i.e. at a quite late stage, at high annealing temperature. This gives rise to compromise structural stages with the formation of several metastable structures. These metastable states are characterized by stress compensation features (dislocations, pyramids, and ripples) because the altered composition of the surface region leads to reduced lattice constants. Indeed, a quantitative study by means of Monte Carlo simulations lead to the conclusion that the $Pt_3Sn(111)$-$(\sqrt{3}\times\sqrt{3})$ R30°surface is a consequence of a restricted, local equilibrium in the surface region [79]. Such behavior is in contrast to alloy surfaces where the segregating and the preferentially sputtered species differ, e.g. $Au_{75}Pd_{25}$ [28]. A thermal equilibrium can be even completely out of reach if the sublimation energies differ largely. The latter was observed with Fe-Al alloy surfaces where at the temperature that is necessary to restore the surface composition severe evaporation of Al takes place [80]. With Pt-Sn surfaces no significant evidence of Sn for sublimation has observed: However, on the $Pt_3Sn(110)$ surface mobile monolayer-deep depressions have been observed at Sn-positions in the topography which are most likely vacancies left after sublimation of Sn atoms. The high cohesion of heterogeneous bonds prevents that Pt atoms jump in these vacancies at Sn positions.

Although these simple considerations help to frame in a general logic the behavior of these bimetallic surface, there are at present no such simple models to explain the more complex "mesoscopic" reconstructions, such as the "pyramids" observed on $Pt_3Sn(100)$ or the hill and valley structure observed on $Pt_3Sn(110)$. These phenomena are obviously related to the tendency of the system to relax in-plane stress, in turn resulting from the different atomic radius of the elements involved in the presence of concentration gradients. This relaxation appears to take place on the (111) oriented plane simply by an outward relaxation of the tin atoms. On the other two low index surfaces, instead, it takes a more complex route leading to reconstruction phenomena (pyramids on the (100) and "hill and valley" on the (110)) which are so far unique to the Pt-Sn system.

4.2 Defects and disorder on Pt_3Sn alloy surfaces

The field of atomic scale defects on alloy surfaces is one that has recently received a strong inpulse by STM studies. Nevertheless, also classic crystallo-

graphic techniques can be used to study defects. Ordered step arrays of alloy surfaces can be studied by LEED ($Pt_3Ti(510)$ [81, 82], by LEIS (AlNi(111), [83], and it has been shown how it is possible to detect a stacking fault by XPD during the growth of a metal overlayer (Ag deposited on Pd(111) [84]). Quantitative LEED crystallography has also been used to study the effect of ion bombardment on the composition of alloy surfaces (the case of FeAl(100), [85]). However, STM has the unique capability of imaging defects in real space. So it is possible, for instance, to observe the step distribution and height on the surface (one of the first reports in this field was on the NiAl(111) surface [86]). Later on [87, 88] it was observed by STM that ion bombardment of the $Pt_{25}Ni_{75}(111)$ surface leads to the formation of a pattern of shallow ditches (some 0.2-0.5 Å deep) that have been attributed to the dislocations generated by the lattice mismatch of the top layers and the bulk ones. The top layers are enriched in Pt by ion bombardment and hence have a different lattice constant. These dislocations in sputtered alloys may provide diffusion pipes for implanted atoms to reach the surface. Diffusion of metal atoms in the surface region at relatively low temperatures has however been proven to be related to the presence of defects, such as the "pinholes" observed by STM at the Co/Cu(100) interface [89]

The study of the $Pt_3Sn(111)$ surface by STM has expanded and clarified this area. Here the mesoscopic "honeycomb" structure reported in [35] is something that finds a parallel only in the case of the Pt-Ni system [87, 88]. In both cases, the surface develops mesoscopic features which are due to lattice dislocations in turn due to the composition gradient in the direction perpendicular to the surface. In the case of the $Pt_3Sn(111)$ system, the depletion in the subsurface which is associated with the formation of the $(\sqrt{3} \times \sqrt{3})$ R30°structure leads to a lattice constant in that region which can be expected to approach the Pt bulk lattice constant of 3.92 A. This value is lower than the Pt_3Sn bulk lattice constant of 4.00 A. This mismatch of the lattice constants causes tensile stress which is obviously relieved by misfit dislocations. Additionally, stress relief may be the cause of the slight buckling of the Sn atoms on (111) as observed the quantitative LEED analysis [34]. A direct determination of the Burgers vector of the dislocation is not possible since none of them reach the surface. However from the directions of the walls of the honeycombs along 112 we conclude that the Burgers vectors must be parallel to the surface $\frac{1}{2}\ \langle 110 \rangle$. Good alignment of the walls of the network is obtained after annealing slightly above 600 K. The half-width of the walls as obtained from a corresponding cross section is of the order of 30 to 40 A. From this width the depth of the dislocation cores can be estimated to be approximately 15 layers [90]. 15 layers is also the range of Pt enrichment found in previous LEED studies [33] so the results of the

different methods used, LEIS, LEED, XPD, AES and STM, lead to a consistent interpretation of the metastable phase of the $Pt_3Sn(111)$ surface.

At present the case of Pt_3Sn and Pt_xNi_{x-1} are the only two cases reported of STM observations of misfit dislocations resulting in mesoscopic surface features, however it is certain possible that new cases will be discovered as different alloy systems are studied.

4.3 Multilayer and single layer surface alloys

Both single layer and multilayer surface alloys can be prepared in the Pt-Sn system by depositing ultra-thin Sn layers and annealing in vacuum to obtain equilibration. The first case where structural data were reported about a similar phenomenon was for the Al/Ni system [91], where the formation of an eptiaxial Ni_3Al layer was observed when depositing Al on Ni(100). Other case known where this occurs are the Au-Cu(100) [92] and the Pd-Cu(001) [93] systems. In other cases, such as Co-Pt(111) [94], only multilayer surface alloys are known to form, although alloying appears to be limited to the outermost 2 surface layers only. So far, the structure of most of these surface phases turned out to be the one that maximizes the number of heterogeneous pairwise interactions. Qualitatively, the expectation is that such phases would be stabilized by a strong intermetallic bond and hence, exist for elements that form ordered bulk alloys, or anyway alloys with a negative enthalpy of formation.

The general explanation for the existence of single layer surface alloys appears to lie in the balance of tendencies that are usually opposite: that of maximizing the number of energetically favorable intermetallic bonds, and that of minimizing surface energy. The maximization of the number of bonds, alone, would necessarily lead to long range bulk diffusion and to the formation of a dilute bulk alloy. However, placing the minority component within the topmost surface layer only may be energetically favorable in several ways; for instance relieving strain effects due to size differences. As already discussed for the case of diluted bulk alloys, the stability of single layer alloy phases can be theoretically predicted, for instance by the EAM theory [78] or by the TBIM approach [95, 96, 97, 98]. In the case of the Cu/Au(111) system the EAM theory predicts that a gold atom placed within the first atomic layer in the c(2x2) phase is 0.14 eV more stable than as an adatom. The stability of the W(100) c(2x2)-Cu phase has been explained in terms of the energetic contribution of the lattice strain of the overlayer to the overall energy of the system [99]. The case of the incorporation of gold atoms in the Ni (110) plane (Fig. 7) could be theoretically explained in the framework of the EMT theory (Effective Medium Theory) [100], that indicates that the surface energy of the Ni(110) surface is lower when Au is incorporated into the first layer. It could be shown that the

cohesive energy of the system has a minimum when Au is surrounded by a low number of Ni neighbors (6-7), as it occurs in a flat surface layer. Similar factors are at play in the case of the Pt-Sn system as discussed by [7].

The stable phase at the Sn/Pt(111) interface after extended thermal treatment at high temperature is the $(\sqrt{3}\times\sqrt{3})$ R30°single layer surface alloy. Its stability can be explained in terms of the surface free energy and the atomic size of Sn and Pt, tin is expected to segregate onto the surface of platinum. On the other hand, a high surface concentration of tin is not a stable situation due to the reduction of the number of favorable Pt-Sn bonds. The single layer Pt(111)$(\sqrt{3}\times\sqrt{3})$ R30°-Sn phase results from the balance of these two contributions, since this phase maximises both the surface concentration of Sn (1/3 of a ML) and the number of Pt-Sn bonds (6 Pt first nearest neighbors). The formation of the $(\sqrt{3}\times\sqrt{3})$ R30°surface alloy by annealing at 1000 K of indicates that diffusion of Sn into the bulk is effective at such a temperature and that equilibrium can be achieved. The conditions of formation of this alloy on the pure Pt(111) surface parallel exactly those of the Pt_3Sn(111) compound. In the latter case, the $(\sqrt{3}\times\sqrt{3})$ R30°reconstruction can be prepared only after a depletion in tin of the subsurface layers is obtained by ion bombardment so that, eventually, the two systems have the same composition and structure over the first few atomic layers from the surface.

In terms of multilayer surface alloys, the deposition of multi-atomic layers of tin on a platinum substrate can lead to the formation of multi-layer surface alloys. The observation of a well defined periodicity in LEED for the Sn/Pt(111) system and the parallel indications of the presence of tin in the subsurface in amount corresponding to approximately 25 at% indicates that we have a true ordered compound which extends for several atomic layers [37]. This behavior appears to be similar to that of the Co-Pt system [94], although in the case of Sn-Pt it was not possible to evidence the same kind of sharp alloy/substrate interface reported for Co/Pt(111). The possibility of obtaining a compound with negative enthalpy of formation is surely a factor favoring the formation of a multilayer homogeneous alloy in this sytem however, in this as in other systems, kinetic factors may be more important, and in particular factors related to the presence of grain boundaries in the deposited film. The bulk diffusion vacancy mechanism at the temperatures at which multilayer alloy phases have been observed to form are orders of magnitude too slow to cause a significant deep layer diffusion. For instance, the diffusion depth for the case of the Fe-Cu system was estimated as 10-3 Å in the conditions in which a multilayer surface alloy was observed [101]. Egelhoff [102, 103] found that surface mixing in the Cu/Ni system occurs rapidly at temperatures for which the bulk diffusion coefficients lead to predict parameters such as one atomic “hop” (site exchange)

every 1010 years. Clearly, other mechanisms are at play in this area and the only possible conclusion is that diffusion proceeds in these conditions from the substrate into the deposit, exploiting surface defects and imperfection in the deposited film. Substrate diffusion into the deposit has already been experimentally observed for relatively thick In films on Ag [104]. In 1989 Egelhoff [103] predicted that for very thin deposited layers such diffusion would occur via "pits" on the surface, and such pits have been indeed recently observed by STM in the Co/Cu system [89, 105]. ICISS has also provided evidence that diffusion in the Fe/Cu(100) system occurs only in a very small fraction of the area of the surface [106]. Although the diffusion coefficient of Sn in Pt is not known, considering the bulk diffusion coefficient of other metals in platinum Sn diffusion into the Pt substrate should be negligible in a such temperature range [37], so that the mechanism of alloying appears to be dominated here, too, by surface diffusion of Pt atoms through defects of the Sn film. However, the mechanisms of diffusion in these systems, as well as in the Pt-Sn one is something that still needs to be studied in detail.

5. CONCLUSION

The present review has attempted to summarize the experimental observations available for the surface structure of the Pt-Sn system for both single crystal Pt_3Sn samples and for systems obtained depositing and thermally equilibrating tin onto pure Pt surfaces. In many ways, the results obtained for this alloy indicate structural phenomena comparable with those available for other bimetallic system. Several of these results can be explained in terms of well known properties of compounds with a negative enthalpy of formation, which tend to form structures which maximize the number of heterogeneous pairwise interactions. At the same time, other factors related at least in part to atomic size tend to influence the surface structure by stabilizing or de-stabilizing mixed topmost layer. In the case of Pt-Sn these factors lead to the formation of stable and well characterized surface phases, such as the $(\sqrt{3}\times\sqrt{3})$ R30°-Sn which can be obtained starting from either single crystal Pt_3Sn or from the deposition of Sn on pure Pt(111). This phase is one of the best known and understood "model" for gas-solid interactions which examine how chemisorption, gas phaser catalytic and electrocatalytic reactions can be affected by sterical factors, site availability, and at the same time by electronic deinsity variations resulting from the intermetallic bond. In this area, the behavior of the Pt-Sn system sharply contrast with that of other platinum -metal systems (with the second metal, for instance, Co, Ni, Ti) where there exists a strong tendency for platinum to segregate and to form what may be called "skin" alloy surfaces [5].

Although simple, flat surface phases are observed, the Pt-Sn system is also remarkable for the complexity of mesoscopic phenomena observed, such as the "pyramids" formed on the $Pt_3Sn(100)$ surface. These phenomena are obviously related to the high surface energy of the system, which is possibily the intermetallic compound with the largest enthalpy of formation studied so far for its surface properties. No comparable phenomena have been observed in other bimetallic systems so far.

The field of alloy surfaces has undergone remarkable advances in the last few years, in large part pushed by the application of atomic resolution real-space imaging techniques. The wealth of observations on the Pt-Sn system can be considered as a starting point for a more complete assessment of this vast field.

APPENDIX: NOTES ON NOMENCLATURE

Some nomenclature problems general to alloy surfaces and specific for the Pt-Sn system will be briefly reviewed in this section, a more detailed discussion can be found in [5]. The first point to be considered is the form of writing of the alloy composition. In metallurgy it is customary to write the elements of an alloy in order of decreasing atomic fraction. This custom contrasts with the recommendation for intermetallic compounds of the international union for pure and applied chemistry[107]. In the IUPAC rules, elements in intermetallic compound should be ordered in the same way as in inorganic compounds, that is following columns in the periodic table from the bottom up, and rows from left to right. This rule is somewhat cumbersome to follow and it is almost never used for alloys. In most cases (and in the present paper) the metallurgic convention is used and it is probably the best way, that is writing, "Pt_3Sn" rather than the IUPAC style "$SnPt_3$" Elements in "systems" in general can be written simply in alphabetic order (e.g. "the Pt-Sn system").

Another nomenclature problem is related to the definition of surface periodicities. In surface studies the periodicity of the surface unit mesh should be described using the Wood notation [108]. According to this notation, a surface phase is described according to its periodicity referred to that of the substrate. That is, a surface phase which has a unit mesh twice larger than that of the substrate and aligned in the same direction is defined as a "2x2" In the case of binary alloys, when an ordered intermetallic compound (such as Pt_3Sn) is cut along a surface plane, the resulting 'bulk truncation' or 'expected' periodicity should be described as a 1x1 according to the Wood convention. Nevertheless this is practically never done in the literature for binary alloy systems; it is preferred instead to index the surface mesh in terms of a superlattice mesh referred

to one of the two pure components (platinum in the case of Pt_3Sn). This notation is formally incorrect since what is described as a 'surface mesh' is in reality the periodicity of the bulk lattice, not that of the surface or selvedge. Nevertheless, the 'superperiodicity' notation is almost impossible to avoid in order to describe, for instance, the order-disorder ($2x2 \leftrightarrow 1x1$) transition that occurs in Cu_3Au. Otherwise one would have to modify the periodicity notation for the overlayer depending on the order/disorder state of the substrate which would lead to considerable confusion when comparing, for instance, identical structures formed starting from intermetallic bulk compounds or instead by deposition of tin metal on a bulk platinum substrate.

REFERENCES

[1] Campbell C. T., Ann. Rev. Phys. Chem. 41 (1990) 775.

[2] Nieuwenhuys B.E., in The Chemical Physics of Solid Surfaces and Heterogeneous Catalysis, Eds. King, DA and Woodruff, DP), Elsevier, Amsterdam, 1993, Vol. 6, pp. 185-224.

[3] Wandelt K., in "Surface Science, Principles and Applications, Springer Proceedings in Physics, Vol 73, R.F. How, R.N. Lamb and K. Wandelt eds, Springer Verlag, Berlin Heidelberg, 1993, 209-226.

[4] Prasad B.D., Sankaran S.N., Wiedemann K. E., Glass D.E. Thin Solid Films 345 (1999) 255.

[5] Bardi U., Rep. Prog. Phys. 57 (1994) 939.

[6] Vasiliev M.A. J Phys. D Appl. Phys. 30 (1997) 3037.

[7] Treglia, G., Legrand B., Ducastelle F. , Saul A., Gallis G., Meunier I., Mottet C., Senhaji A. Computational Materials Science 15 (1999) 196.

[8] Rodriguez, J. A., Surf. Sci. Rep. 24 (1996) 223.

[9] Christensen A., Ruban V., Stolze P., Jacobsen K.W., Skriver H.L., Norskov J.K., Besenbacher F., Phys. Rev. B 56 (1997) 5822.

[10] Brewer L. in "Phase stability in Metals and alloys" Eds. P. Rudman, J,. Jaffee and R.I. Jafee, McGraw Hill New York, 1967.

[11] Hayer E. Bros J.P., J. Alloys Com. 220 (1995) 193.

[12] Abdel-Rahim M.A., Khalil M.W., Hassan H.B., J. Appl. Electrochemistry 30(10) (2000) 1151.

[13] Burch R., J. Catal. 71(1981) 348.

[14] Anres, P, Gaine-Escard, M.. Bros, J.P., Hayer E., Journal of alloys and compounds 280 (1998) 158.

[15] Van Hove M. A., Weinberg W. H., Chan C. M., Springer Series in Surface Science, Berlin -Heidelberg 1986.

[16] Gauthier Y., Baudoing R., in "Surface segregation and related phenomena, Eds. P.A. Dowben, A. Miller, CrC press, Boca Raton, 1990, p. 169.

[17] Atrei A., Bardi U., Rovida G., Torrini M., Zanazzi E., Ross P. N., Phys. Rev. B46 (1992) 1649.

[18] Ceelen, W.C.A.N., Denier van der GonA.W., Rejime M.A., Brongersma H.H., Spolveri I., Atrei A., Bardi U., Surf. Sci. 406 (1998) 264.

[19] Fadley C. S., Prog. Surf. Sci. 16 (1984) 275.
[20] Bardi U., Pedocchi L., Rovida G., Haner A. H., Ross P. N., In Fundamental aspects of heterogeneous catalysis; H.H. Brongersma, R.A. van Santen eds, Plenum Press, New York, 1991, 393.
[21] Overbury S. H., Ku Y., Phys. Rev. B46 (1992) 7868.
[22] Overbury S. H., van den Oetalaar R. J. A., Zehner D. M., Phys. Rev. B 48 (1993) 1718.
[23] Li Y., Koel B.E., Surf. Sci. 330 (1995) 193.
[24] Niehus H., Achete C., Surf. Sci. 289 (1993) 19.
[25] O'Connor D.J., Shen Y.G., Zur Muhlen E., Zhu L., Macdonald R.J., Surf. Rev. Letters 3 (1996) 1847.
[26] Varga P., Schmid M., Appl.Surf.Sci. 141 (1999) 287.
[27] Hoheisel M., Kuntze J., Speller S., Postnikov A., Heiland W., Spolveri I., U. Bardi, Phys. Rev. B 60 (1999) 2033.
[28] Aschoff M., Speller S., Kuntze J., Heiland W., Platzgummer E., Schmid M., Varga P., Baretzky B., Surf. Sci. 415 (1998) L1051.
[29] Tsong T.T., Müller E.W., Journ. Appl. Phys. 38 (1967) 3531.
[30] Haner A. N., Ross P. N., Bardi U., Catalysis Lett. 8 (1991) 1.
[31] Haner A. N., Ross P. N., Bardi U., 1991 The structure of Surfaces III; S.Y. Tong, M.A. Van Hove, K. Takayanagi, X.D. Xie eds, Springer Verlag, Berlin Heidelberg, 24 276-281.
[32] Haner A. N., Ross P. N., Bardi U., Surf. Sci. 249 (1991) 15.
[33] Atrei A., Bardi U., Zanazzi E., Rovida G., Kasamura H., Kudo M., J. Phys. Condens. Matter 5 (1993) L207.
[34] Atrei A., Bardi U., Wu J. X., Zanazzi E., Rovida G., Surf. Sci. 290 (1993) 286.
[35] Kuntze J, Speller S., Heiland W, Atrei, A., Spolveri I., Bardi U., Phys. Rev. B 58 (1998) R16005.
[36] Hoheisel M., Speller S., Heiland W., Atrei A., Bardi U., Rovida G., submitted to Phys. Rev. B.
[37] Galleotti M., Atrei A., Bardi U., Rovida G., Torrini M., Surf. Sci. 313 (1994) 349.
[38] Maclaren J. M., Surface Crystallographic Handbook (Dordrecht) (1987).
[39] Koch R., Borbonus M., Haase O., Rieder K.H., Phys. Rev. Lett. 67 (1991) 3416.
[40] Hoheisel M., Speller S., Kuntze J., Atrei A., Bardi U., Heiland W., Phys. Rev. B63 (2001) 245403.
[41] Niehus H., Heiland W., Taglauer E, Surf. Sci. Rep. 17 (1993) 213.
[42] Paffett M.T, Windham R.G., Surf. Sci 208 (1989) 34.
[43] Overbury S. H., Mullins D. R., Paffett M. F., Koel B. E., Surf. Sci. 254 (1991) 45.
[44] Batzill M., Beck D.E., Koel B.E., Surf. Sci. 466 (2000) L821.
[45] Xu C., Koel B.E., Surf. Sci. Lett. 304 (1994) L505.
[46] Xu C., Peck J.W., Koel B.E., J. Am. Chem Soc. 115 (1993) 80.
[47] Xu C., Tsai Y.L., Koel B.E., J. Phys. Chem. 98 (1994) 585.
[48] Xu C., Koel B.E., Surf. Sci. 304 (1994) 249.
[49] Xu C., B.E. Koel, Paffett M.T., Langmuir 10 (1994) 166.
[50] Panja C., Saliba N., Koel B.E. Surf. Sci. 395 (1998) 248.
[51] Gallego S., Ocal C., Mendez J., Torrelles X., Soria F., Surf. Sci. 482-485 (2001) 1303.
[52] Sondericker D., Jona F., Marcus P. M., Phys. Rev. B 33 (1986) 900.
[53] Sondericker D., Jona F., Marcus P. M., Phys. Rev. B34 (1986) 6770.
[54] Potter H. C., Blakely J. M., J. Vac. Sci. Technol 12 (1975) 635.

[55] Nakanishi S., Kawamoto K., Fukuoka N., Umezawa K., Surf. Sci. 261 (1992) 342.
[56] Sundaram V. S., Farrel B., Alben R. S., Alben,, Robertson W. D., Phys. Rev. Lett. 31 (1973) 1136.
[57] Sundaram V. S., Alben R. S., Robertson W. D., Surf. Sci. 46 (1974) 653.
[58] Buck T. M., Wheatley G. H., Marchut L., Phys. Rev. Lett. 51 (1983) 43.
[59] McRae E. G., Malic R. A., Surf. Sci. 148 (1984) 551.
[60] Stuck A., Osterwalder J., Schlapback L., Poon H. C., Surf. Sci. 251/252 (1991) 670.
[61] Meschter P.J., Worrell W.L., Metall. Trans. A 7(1976) 299.
[62] Pick S., J Phys. Cond. Matter 5 (1993) 6581.
[63] Pick S., Surf. Sci. 436 (1999) 220.
[64] Paul J., Cameron S. D., Dwyer D. J., Hoffmann F. M., Surf. Sci. 177 (1986) 121.
[65] Atrei A., Pedocchi L., Bardi U., Rovida G., Torrini M., Zanazzi E., Van Hove M. A., Ross P. N., Surf. Sci. 261 (1992) 64.
[66] Chen W., Paul J. A. K., Barbieri A., VAn Hove M. A., Cameron S., Dwyer D. J., J. Phys, Condens. Matter 5 (1993) 4585.
[67] Bardi U., Ross P. N., Somorjai G. A., J. Vac. Sci. Technol. A2 (1984) 40.
[68] Mullins D. R., Overbury S. H., Surf. Sci. 199 (1988) 141.
[69] Beccat P., Gauthier Y., Baudoing-Savois R., Bertolini J. C., Surf. Sci. 238 (1990) 105.
[70] Bardi U., Atrei A., Rovida G., Cortigiani B., Rovida G., Torrini M., Surf. Sci. 282 (1993) L365.
[71] Spencer M. S., Surf. Sci. 145 (1984) 145.
[72] Bardi U., Atrei A., Ross P. N., Zanazzi E., Rovida G., Surf. Sci. 211/212 (1989) 441.
[73] Van Hove M. A., Koestner R. J., Stair P. C., Biberian J. P., Kesmodel L. I., Bartos I., Somorjai G. A., Surf. Sci. 103 (1981) 189.
[74] Baird R. J., Eberhardt W., J. Vac. Sci Technol. 18 (1981) 538.
[75] Baird R. J., Ogletree D. F., Van Hove M. A., Somorjai G. A., Bull. Am. Phys. Soc. 29 (1984) 222.
[76] Baird R. J., Ogletree D. F., Van Hove M. A., Somorjai G. A., Surf. Sci. 165 (1986) 345.
[77] Esposto F. J., Zhang C. S., Norton P. R., Timsit R. S., Surf. Sci. 290 (1993) 93.
[78] Foiles S. M., Surf. Sci. 191 (1987) 329.
[79] Creemers C., Helfensteyn S., Appl. Surf. Sci. 167, (2000) 216.
[80] Meier W., Blum V., Hammer L., Heinz K., J Phys. Cond. Mat. 13, (2001) 1781.
[81] Bardi U., Santucci A., Rovida G., Ross P. N., Proceedings of the ICSOS-2, Springer Verlag, Berlin, Heidelberg, New York, London, Paris Tokyo, 1987, 147-151.
[82] Bardi U., Ross P. N., Rovida G., Surf. Sci. Lett. 205 (1988) L798.
[83] Overbury S. H., Mullins D. R., Wendelken J. F., Surf. Sci. 236 (1990) 122.
[84] Eisenhut B., Stober J., Rangelov G., Fauster T., Phys. Rev. 47 (1993) 12980.
[85] Wang C. P., Jona F., Gleason N. R., Strongin D. R., Marcus P. M., Surf. Sci. 298 (1993) 114.
[86] Niehus H., Raunau W., Besoche K., Spitzl R., Comsa G., Surf. Sci Lett. 225 (1990) L8.
[87] Schmid M., Biedermann A., Stadler H., Slama C., Varga P., Appl. Phys. A55 (1992) 468.
[88] Schmid M., Biedermann A., Stadler H., Varga P., Phys. Rev. Lett. 69 (1992) 925.
[89] Schmid A.K., Atlan D., Itoh H., Heinrich B., Ichinokawa T., Kirschner J., Phys. Rev. B. 48 (1993) 2855.
[90] Stalder R., Sirringhaus H., Onda N., von Känel H., Appl. Phys. Lett. 59 (1991) 1960.

[91] Lu S. H., Tian D., Wang Z. Q., Li Y. S., Jona F., Marcus P. M., Solid state Comm. 67 (1988) 325.
[92] Naumovich D., Stuck A., Greber T., Osterwalder J., Schlapbach L., Surf. Sci. 269/270 (1992) 719.
[93] Lu S. H., Wang Z. Q., Wu S. C., Lok C. K. C., Quinn J., Li Y. S., Tian D., Jona F., Marcus P. M., Phys. Rev. B37 (1988) 4296.
[94] Galeotti M., Atrei A., Bardi U., Cortigiani B., Rovida G., Torrini M., Surf. Sci. 297 (1993) 202.
[95] Teraoka Y., Surf. Sci. 232 (1990) 193.
[96] Teraoka Y., Surf. Sci 235 (1990) 208.
[97] Teraoka Y., Surf. Sci 235 (1990) 249.
[98] Teraoka Y., Surf. Sci 238 (1990) L453.
[99] Singh D., Krakauer H., Surf. Sci. 216 (1989) 303.
[100] Jacobsen K. W., Norskov J. K., Puska M. J., Phys. Rev. B35 (1987) 7423.
[101] Thomassen J., May F., Feldmann B., Wuttig M., Ibach H., Phys. Rev. Lett. 69 (1992) 3831.
[102] Egelhoff W.F., J. Vac. Sci. Technol. A7 (1989) 2060.
[103] Egelhoff W.F., Steigerwald D.A., J. Vac. Sci. Technol. A7 (1989) 2167.
[104] Wesche R., Fink R., Krausch G., Platzer R., Voigt J., Wohrmann U., Schatz G., Thin Solid Films 190 (1990) 153.
[105] Girgel J., Kirschner J., Landgraf J., Shen J., Woltersdorf J., Surf. Sci. 310 (1994) 1.
[106] Detzel Th., Memmel N., Phys. Rev. B 49 (1994) 5599.
[107] IUPAC, J. Am. Chem. Soc. 82 (1960) 5525.
[108] E.A.Wood, Crystal Orientation Manual, Columbia University Press, New York and London, 1963.